Ray Casting based Correction Algorithm

for

Terahertz Non-Line-of-Sight Imaging

by

Shanmukha Saketha Ramanujam Samavedam

A Thesis Presented in Partial Fulfillment
of the Requirements for the Degree
Master of Science

Approved April 2024 by the
Graduate Supervisory Committee:

Georgios Trichopoulos, Chair
Ahmed Alkhateeb
Seyedmohammadreza Faghih Imani

ARIZONA STATE UNIVERSITY

May 2024

ABSTRACT

Traditional imaging systems such as the human eye and optical cameras capture the scene ahead of them called the line of sight (LoS) objects. These imaging systems are limited by their lack of field of view (FoV). Information about the non-line of sight (NLoS) objects is lost due to the objects in the LoS. They are either opaque or absorb all the incident energy, allowing for no information about the NLoS scene to be transmitted back to the detector. Amongst the popular methods used for NLoS imaging, acoustic imaging [8] offers low resolutions and suffers from interference from environmental factors. Optical methods like time-of-flight (ToF) imaging perform poorly due to shorter wavelengths leading to more scattering and absorption by occluding objects in the scene. NLoS imaging with electromagnetic (EM) rays is preferred over traditional methods because of its allowance for higher spatial resolution. It is subject to lesser interference by atmospheric factors (wind, temperature gradients.)

Most everyday surfaces offer diffuse and specular reflection due to their material properties. They behave as lossy mirrors enabling propagation paths between a Terahertz (THz) Imaging System and the NLoS objects. THz waves (300 GHz – 10 THz) are the least explored if not exploited band of frequencies in the EM spectrum. A THz NLoS Imaging system is a Radar (Radio Detection and Ranging) that works by recording the backscatter information received from sending out EM signals into free space where the EM signals undergo multiple bounces off different objects in the scene. Due to the inherent nature of the radars, the return information is perceived in a way that the NLoS objects are improperly depicted when reconstructed.

A correction algorithm to account for this misplacement in the reconstruction of NLoS images is proposed and its implementation is discussed in detail as a part of this work. The reconstruction algorithm processes the obtained raw THz image and performs multiple stages of classification between LoS and NLoS objects using ray casting [5]. Then the information about line-of-sight objects is fed to a line detection mechanism to detect and model the detected surfaces as mirrors. Mirror folding [1] is performed starting from the farthest generations for the objects in non-line of sight. This algorithm has been evaluated with simulated images of objects behind a single wall and two walls. With the help of a scanning THz imaging system, measurements were collected in a controlled environment, and this data was fed into the implemented algorithm for testing.

To my parents, teachers, and friends.

Ad Astra Per Aspera

ACKNOWLEDGMENTS

Firstly, I express immense gratitude to Prof. Georgios C. Trichopoulos for his invaluable guidance, mentorship, and guidance throughout this work. Without his expertise and insightful advice, this thesis would not have been possible. I am grateful to the members of the committee, Dr. Ahmed Alkhateeb and Dr. Seyed Mohammadreza Faghih Imani for their constructive criticism and valuable suggestions.

I would also like to thank the senior members and colleagues at the lab, Yiran Cui, Bharath Kashyap, Syam Prakash, and Aditya, for helping me figure my way out with various instruments at the lab and making me feel included. To my friends Abi, Nikhil Srinivas, Pankhuri, and Sankara Dinesh, and my managers Sivaprakash Murugesan and Rui Moreira at Tesla Motors, your support during this work is invaluable.

And to my parents, thank you for supporting me through all my decisions and endeavors.

TABLE OF CONTENTS

Page

CHAPTER Page

LIST OF TABLES

Table Page

LIST OF FIGURES

Figure Page

Figure Page

CHAPTER 1

INTRODUCTION

NLoS Imaging is the method of identifying hidden scenes around an obstacle, for example, a corner by indirectly illuminating the hidden scene with a suitable source and reconstructing the information obtained at the detector using appropriate image reconstruction algorithms. This idea of leveraging the indirect path of propagation of information from the line-of-sight surfaces, to obtain information about objects in the Non-Line of Sight domain of the detector is growing in popularity. The information about the object in the NLoS is collected using the wave reflections from the nearby surfaces that establish the indirect path of propagation. This kind of imaging can be useful in several areas, for example, a.) Simultaneous Localization and Mapping (SLAM) is an area where the usage of Non-Line of Sight (NLoS) imaging can be used for efficient indoor navigation, localization, and tracking. b.) It can be used in collision avoidance in robotic and autonomous driving environments. As is, due to the nature of how the imaging is performed and processed, this imaging information cannot be directly used and needs further improvement. The implementation of one such image reconstruction algorithm is discussed in detail as a part of this research. In this work, we focus on the reconstruction of imaging information obtained in the THz frequencies.

1.1 Motivation and Current Techniques

Imaging is the concept of reproduction of an object's form for visual representation. Imaging systems thus used to capture and reproduce the visual representation are broadly classified into passive and active systems depending on how they illuminate their targets.

Passive imaging refers to the process of generating images without actively emitting any form of energy or radiation to illuminate the target or the subject of the image, instead by relying on ambient sources of radiation such as reflections due to natural light, thermal radiation emitted by objects, etc., Cameras that are commonly used to capture images are considered passive imagers because they only capture the subject based on the light reflected onto the sensor from the background. Active imaging is where the imaging system emits energy, usually in the form of light, sound, or electromagnetic waves to illuminate a subject or the target. LIDARs, RADARs, and acoustic imaging fall under active imaging.

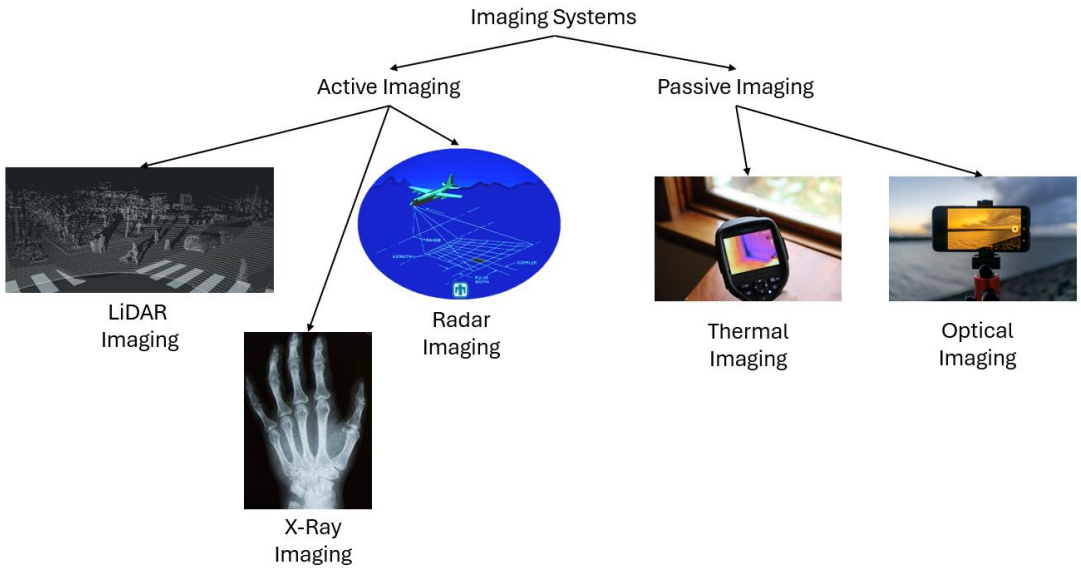

Figure 1-1: Classification of imaging systems, active imaging, passive imaging.

Another classification in imaging is based on the type of objects or targets that are imaged. Objects that are directly in front of the imaging system can be termed line of sight (LoS) objects. Objects that are partially occluded by reflecting surfaces, not in the direct line of the imager, are termed non-line of sight (NLoS) objects.

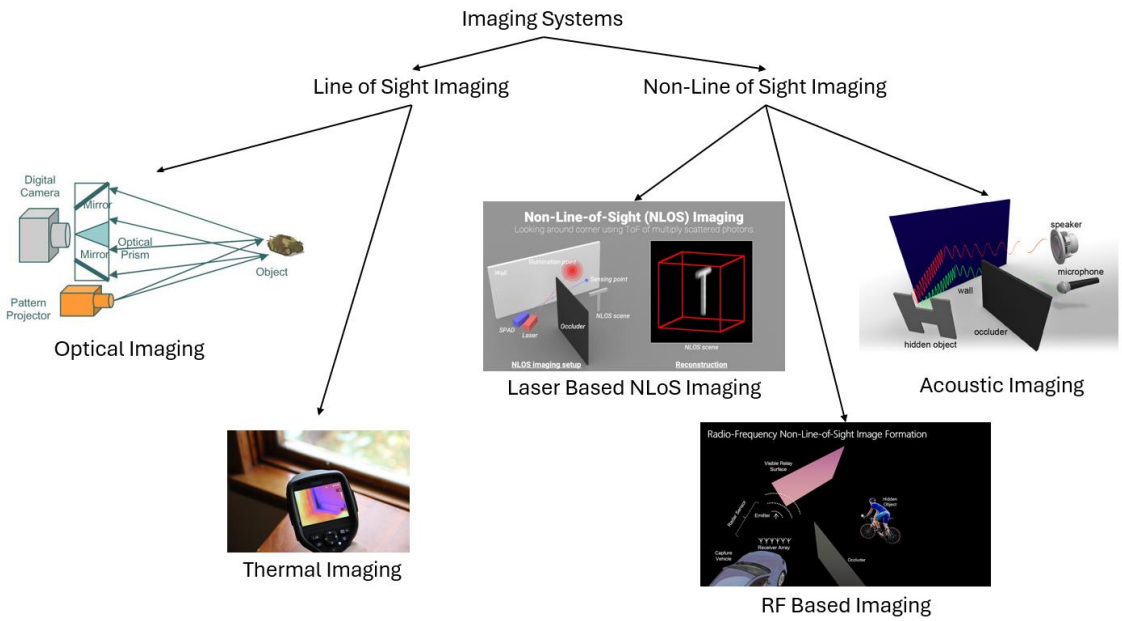

Figure 1-2: Classification of imaging systems, LoS imaging, NLoS imaging

Often, passive imaging systems only capture objects that are in their direct line of sight without the presence of mirrors. Active imaging systems employ a variety of hardware elements, for example, arrays of lasers, photodetectors, microphone arrays, antenna arrays, and microwave transceivers to capture NLoS objects. Capture of NLoS objects is done by utilizing the properties of materials around them and relying on information carried back to the imaging system by wavefronts reflected from the surfaces in the vicinity of the objects in the NLoS region. The return signal's amplitude and phase information are processed to reconstruct the positions of the NLoS objects.

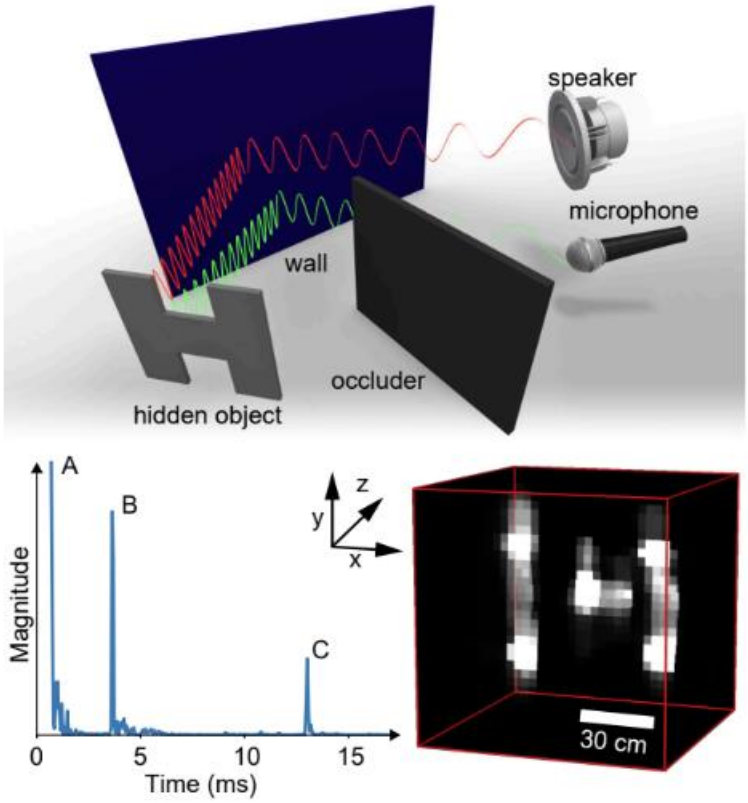

Figure 1-3: Overview of acoustic NLoS imaging [8]

NLoS Imaging employing the idea of acoustics has been demonstrated in [8] where low-cost microphones and speakers are used to image and resolve 3-D shapes around the corners. This technique relies on the idea that the walls around which the objects are to be captured exhibit specular reflection.

Specular reflection is the idea of a wave being reflected at the same angle from the surface normal as the incident wave. This technique does not employ focusing elements and relies on modeling wave effects for sound propagation as acoustic waves dampen faster and are absorbed in the presence of certain materials like foam etc.,

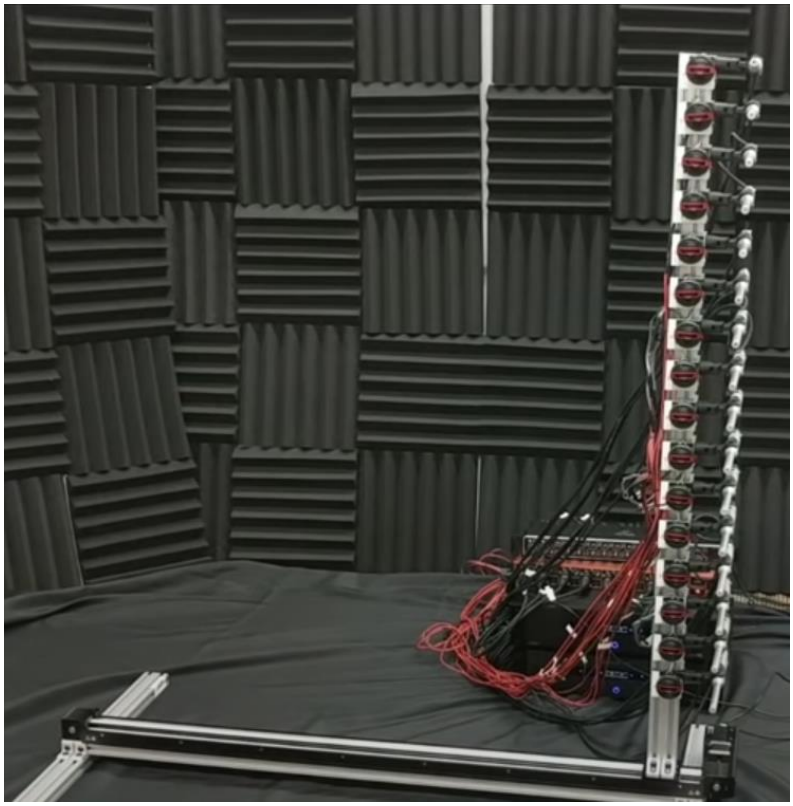

Figure 1-4: Acoustic NLoS imaging setup [8]

As seen above, NLoS imaging setup based in acoustics has a bulky setup including several microphones, speakers, and sound absorbing materials which would be impractical to employ in a typical use case for NLoS imaging that is generally outside where there could be a lot of acoustic noise.

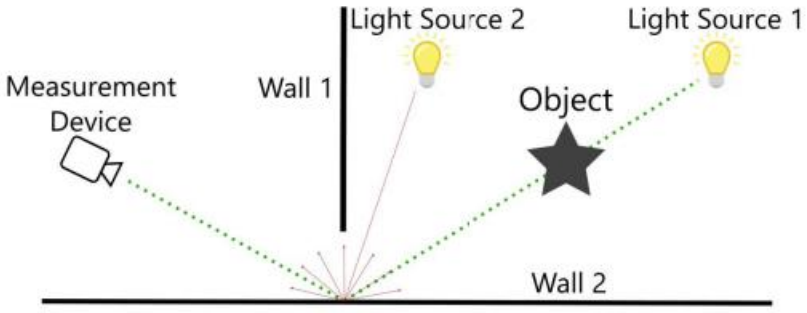

Figure 1-5: NLoS imaging based on diffuse scattering of light.

NLoS Imaging employing light in visible and infrared spectra suffer from diffuse scattering [9] due to surface imperfections leading to the reflected waves having an arbitrary phase at every point on the surface leading to reconstruction errors for NLoS objects. To address the problem of diffuse scattering, high-speed imaging methods using pico-second lasers, time time-resolving cameras have been proposed [18] . The problem with such light-enabled imaging techniques is that they suffer from long integration times, weakly scattered signals, and smaller FoV.

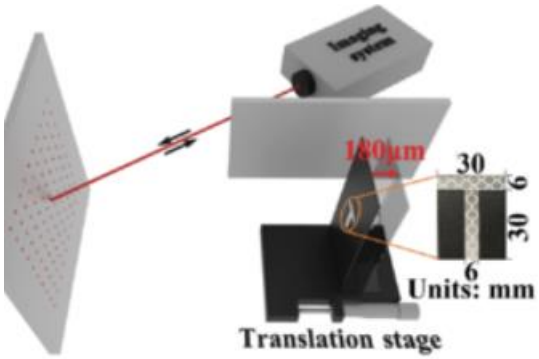

Figure 1-6: Picosecond laser based NLoS imaging system [18].

Imaging techniques that are based on visible, infrared light also suffer from weak backscattering from occluding surfaces, narrower fields of view, and degradation in reconstruction due to multipath losses. [18].

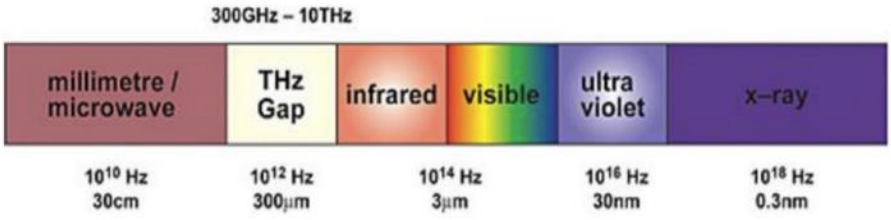

Figure 1-7: Electromagnetic spectrum depicting THz frequencies/wavelengths.

At microwave frequencies, radar imaging techniques are applied to NLoS imaging tasks. While this technique suffers from stronger edge diffractions, semi transparency of materials leading to the cluttering of images due to multipath propagation, THz waves a class of microwave frequencies can be used to overcome the difficulties posed by multipath propagation. THz waves (100 GHz - 10 THz) feature wavelengths of the order of millimeters – sub-millimeters and are strongly reflected in a single direction (specular scattering) by most of the material surfaces in the real world.

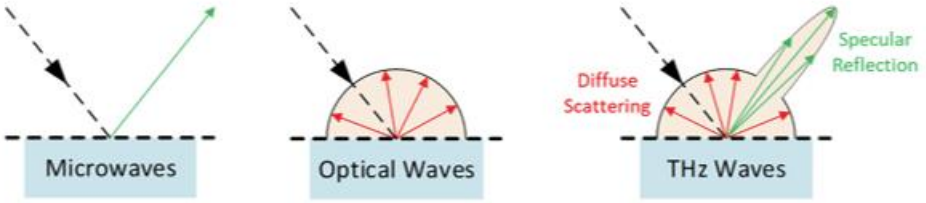

Figure 1-8: Types of reflection occurring in microwaves, optical waves, THz waves [2]

By taking advantage of both specular and diffuse reflections from materials in the real world, THz waves allow for reflecting surfaces to be modeled as lossy mirrors allowing for imaging of NLOS objects from a single observation location. Since the mirroring surfaces are directly in LoS they can be imaged by capturing the backscattered waves (diffuse scattering). This method has been proven to be successful in detecting NLoS geometries.

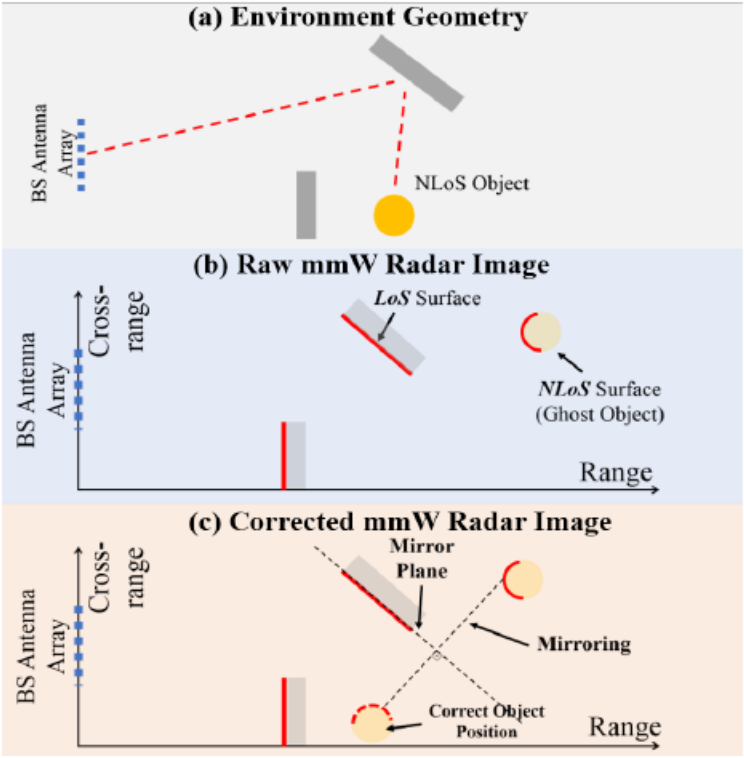

Figure 1.9: Image correction for NLOS objects. (a) Simple topology with two LoS and one NLoS object. (b) NLoS object appears behind the LoS surface in the mm-Wave image (c) Using mirror folding, translation, the NLoS object is placed in the correct position. [3]

While the advantages of imaging NLoS scenarios using THz waves are clear, the images captured by the system need to be corrected to properly account for the errors in the positions of objects in the NLoS domain. This work demonstrates the implementation of a correction algorithm that transforms the raw THz images into the correct geometry. The outline of the algorithm is that the raw data is collected from the imaging system. Ray casting [5] is used to classify LoS and NLoS objects. The classification step can be

applied multiple times to reconstruct multi-bounce scenarios. Probabilistic Hough Line transform is applied to the LoS surfaces to detect the LoS mirror and find its endpoints. The endpoint information generation is used to tag each NLoS object within the field of view (FoV) of a given LoS mirror. Mirror folding is applied to correct the positions of NLoS objects.

1.3 Abbreviations

The abbreviations used in this thesis are summarized in Table 1.1

1.4 Chapter Description

The structure of this document is detailed in the following chapters as

- Chapter 2 describes the ideas of LoS and NLoS imaging in detail, different techniques of imaging in both domains; the Advantages of using THz waves for NLoS imaging, and the need for proper reconstruction algorithms.
- Chapter 3 introduces the ideas of thresholding for the region of interest detection, classification by ray casting, and line detection using hough line transform and geometric transformation to correct a given raw THz imaging scene. The chapter concludes with a breakdown of results obtained on both measured and artificial imaging scenarios.
- Chapter 4 is the closing chapter in this thesis detailing the summary of work, improvements that can be made to the current algorithm.

Table 1.1: Summary of Abbreviations

Acronym	Abbreviation
CCD	Charge Coupled Device
FOV	Field of View
FMCW	Frequency Modulated Continuous Wave
GHz	Giga Hertz (10^9 Hz)
IFT	Inverse Fourier Transform
LiDAR	Light Detection and Ranging
LOS	Line of Sight
MIMO	Multiple Input Multiple Output
NLOS	Non-Line of Sight
RADAR	Radio Detection and Ranging
SLAM	Simultaneous Localization and Mapping
SNR	Signal-to-Noise Ratio
TCP	Transmission Control Protocol
THz	Tera Hertz (10^{12} Hz)
TOF	Time of Flight
USB	Universal Serial Bus
VNA	Vector Network Analyzer

CHAPTER 2

TERAHERTZ AND NON-LIGHT OF SIGHT IMAGING CONCEPTS

2.1 Introduction to THz Imaging

THz bands lie between the microwave and Infrared (IR) frequency bands featuring wavelengths of the orders of 0.03 mm to 3 mm. The THz waves are non-ionizing, non-destructive, and do not penetrate deep into the surface of most materials. The term THz gap (Figure 1-7) indicates this unexplored part of the EM spectrum due to the lack of wide technological and commercial development.

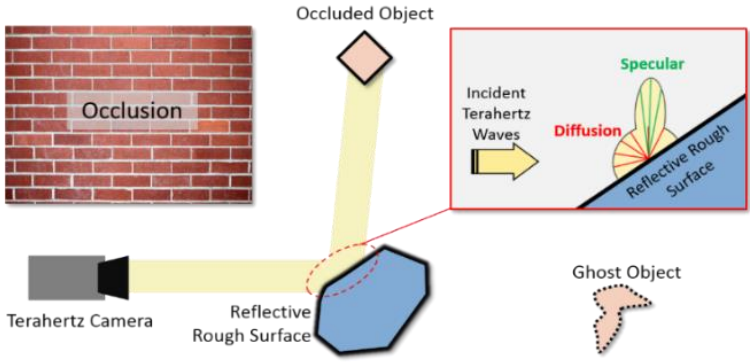

Figure 2-1: Terahertz waves reflect from most building surfaces and enable multipath NLoS imaging under low visibility conditions with compact and portable imaging systems.

Because of their shorter wavelengths, a higher spatial resolution is possible. This is an important feature for imaging. Most of the day-to-day surfaces, like the rough brick walls, and dry walls around which we intend to image the NLoS objects have a surface roughness comparable to the wavelength of THz waves. The problem of some surfaces

not being detected as in the case of highly penetrable microwave frequencies is not present.

2.2 Active THz Imaging (LoS)

2.2.1 Experimental Setup

a.)

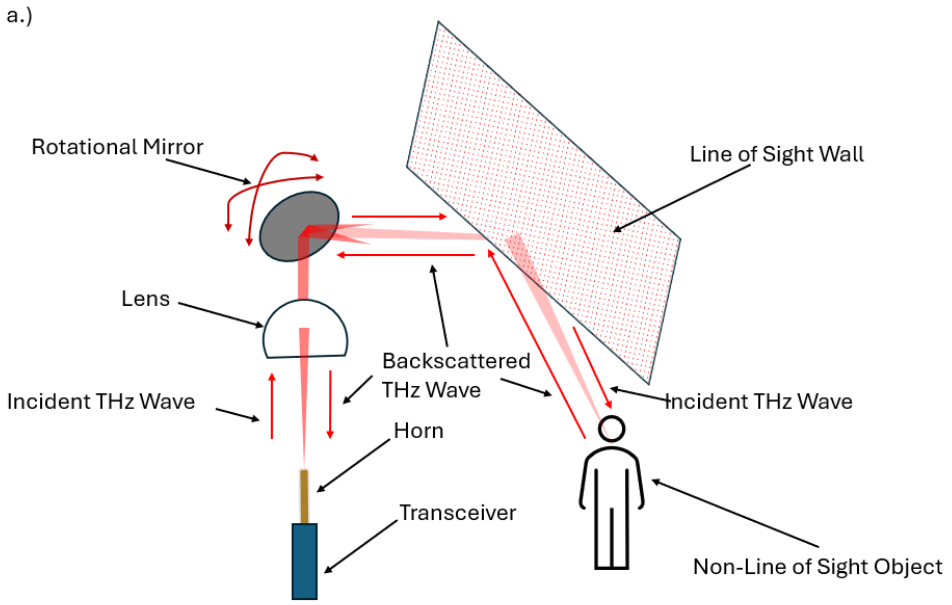

b.)

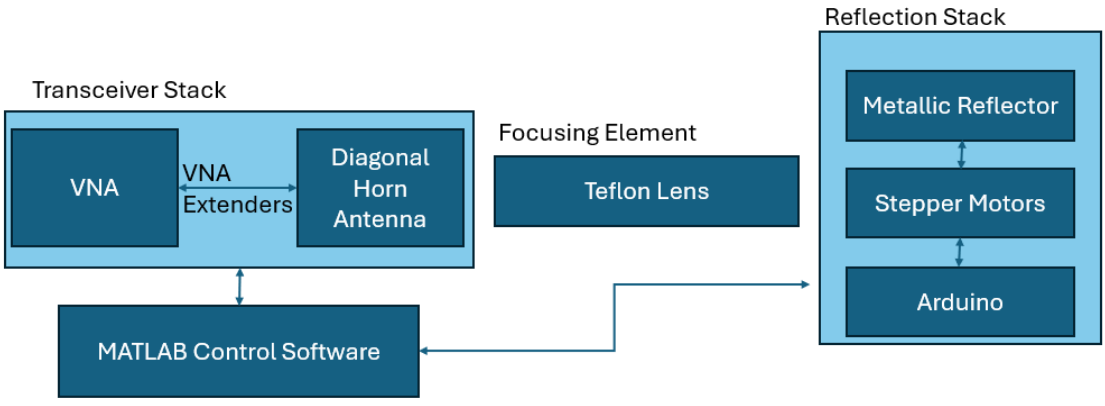

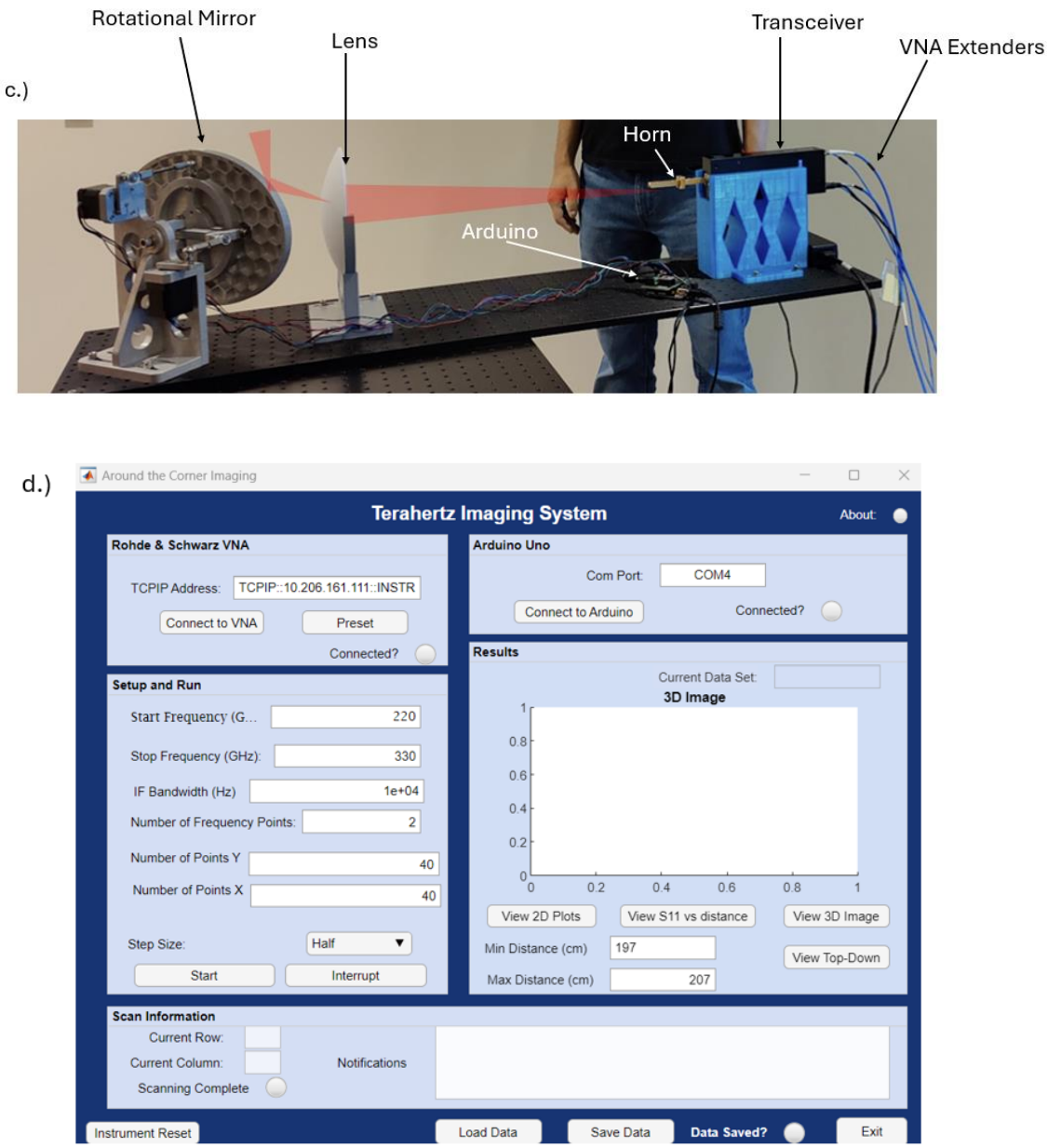

Figure 2-2: Active THz imaging system. a.) Principle of operation of a THz imaging system, showing a single LoS wall and a NLoS object being captured. b.) Block diagram of components in a THz imaging system. c.) Side view of a THz imaging system. d.) Software interface to capture THz image.

Capturing a THz NLoS image requires the scattered signal to be collected across an aperture at distinct positions and the total bandwidth. The process of image capture is performed by a MATLAB application shown in Figure 2-2(d). This interface allows for scanning of the beam in azimuth, elevation, frequency. 3 of these parameters can be controlled independently by changing the values of 'Number of Points Y', 'Number of Points X', 'Start Frequency', 'Stop Frequency' respectively.

As mentioned in section 1.1 active imaging systems generate their illumination to capture the objects in each scene. The THz imaging system contains a single sub-THz transceiver, the Rohde and Schwartz (R&S) VNA coupled with a diagonal horn antenna connected to the transceiver. The transceiver is a VNA extender that measures the S_{11} parameter in the WR3.4 band (220 GHz – 330 GHz). The feed horn has an HPBW of 10^0 and a gain of 26 dB. The imaging system emits a diverging THz beam into the free space. This diverging beam is focused on a translational metallic stage using a custom Teflon lens. The lens is placed 50 cm from the position of the horn and has a focal length of 44.5 cm. This arrangement leads to the THz beam being focused onto a spot with an approximate radius of about 1.7 cm at 3.6 m. The motorized metallic mirror has two stepper motors that can be controlled using the Arduino microcontroller board via the MATLAB interface. The imaging system can form a narrow THz beam with the beam being steerable in the +- 15^o range.

2.2.2 Generating a THz image

We assume this to be an active imaging system where a narrow beam is scanned in both azimuth, elevation directions to obtain the angle-of-arrival (AoA) information of the backscattered signals. At each scanning angle, time-of-flight (ToF) information of the

received signals is also measured. By combining AoA and ToF information, a 3D image of the scene shown as range vs cross range is formed. The 3D image is made of voxels (3D equivalent of a pixel). The brightness of each voxel corresponds to the intensity of the backscattered signal.

For imaging, it is noted that, based on the Rayleigh criterion, the angular resolution is

$$\theta = 1.22\lambda/D$$

where λ is the wavelength of the incident signal, and D is the diameter of the imaging aperture. According to the sampling theorem, the range resolution is given by

$$Range\ Resolution = c_0/(2\beta)$$

where c_0 is the speed of light in free space and β is the bandwidth of the measurement frequency.

The MATLAB script controls the R&S VNA, Arduino to trigger capturing the image and stores the data into a 3D matrix of dimensions N_a x N_e x M where N_a is the number of scanning angles in the Azimuth plane, N_e is scanning angles in the elevation plane, M is the number of discretized frequency points along the range direction. At each scanning angle, the transceiver measures the S_{11} parameter in the frequency domain. Each point in the resulting dataset is a complex-valued voxel which is then converted into a time-domain data point by applying the Inverse Fourier Transform (IFT). This conversion helps obtain the range information based on c_0.

The numerical value assigned to each voxel corresponds to the intensity of the backscattered signals (reflections containing the information about the NLoS object originating from the LoS surfaces back at the transceiver).

Because of the nature of propagation in THz waves, we have an initial image that is an inaccurate depiction of the actual scene. Due to strong specular reflection from neighboring surfaces in the scene, multiple reflections may occur leading to the formation of ghost objects. i.e., the NLoS objects will appear in incorrect poses (position and orientation) at incorrect locations within the raw image. This presents a need for correcting the position of NLoS objects to reposition and reorient them to represent their real-world positions. To perform such a correction, we take the 2D cut of the 3-D image and apply the correction algorithm.

2.3 LoS Image

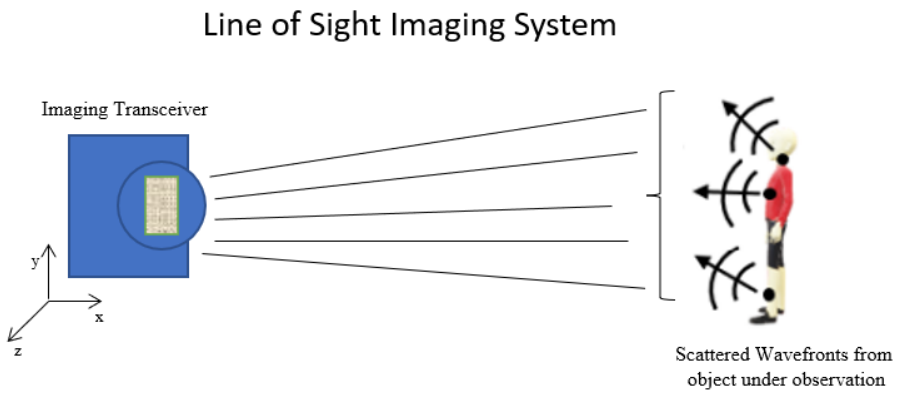

Figure 2-3: Illustration of a Line-of-Sight Imaging System

Shown here is a cartoon of a subject in the LoS of THz camera. The imaging transceiver emits THz waves towards the subject. As there are no strong reflecting surfaces, the reflections from the object in front of the THz camera are scattered directly back to the transceiver. Once processed, we have figure 2-4.

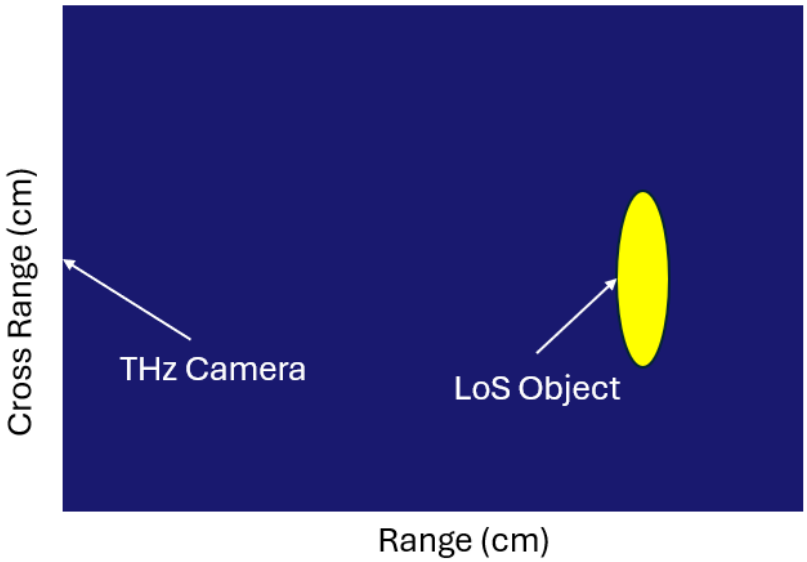

Figure 2-4: Depiction of a LoS object captured by the THz imaging system.

The object in the line of sight is depicted by the bright yellow blob in front of the imaging system. As mentioned previously, this is a 2D cross-section of the 3D scene.

2.4 NLoS Image

An example NLoS image has been captured by placing a mannequin in the hall corridor of a hallway at THz research laboratory. The imaging system is in the hallway facing the walls and a mannequin is placed next to a fire extinguisher box in the corridor. A simple beam scanning is performed with the imaging system capturing the edges of the wall, the NLoS region which is reconstructed in figure 2-5.

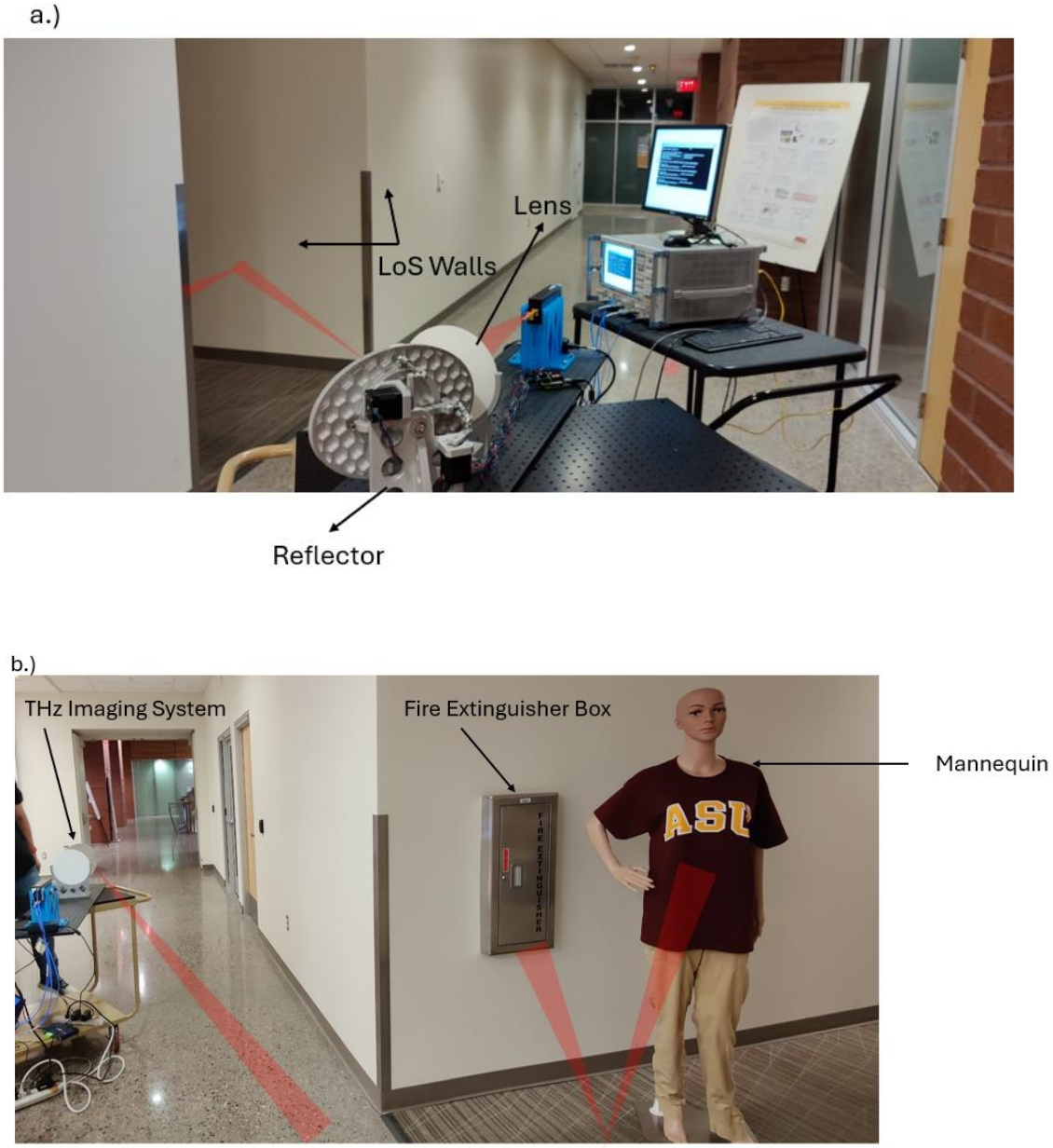

Figure 2-5: A THz Imaging experiment performed with the THz camera facing the wall and a mannequin placed in the NLoS region of the Camera.

a.) THz imaging system facing LoS walls with an edge.

b.) NLoS region representing the presence of a mannequin and a fire extinguisher box.

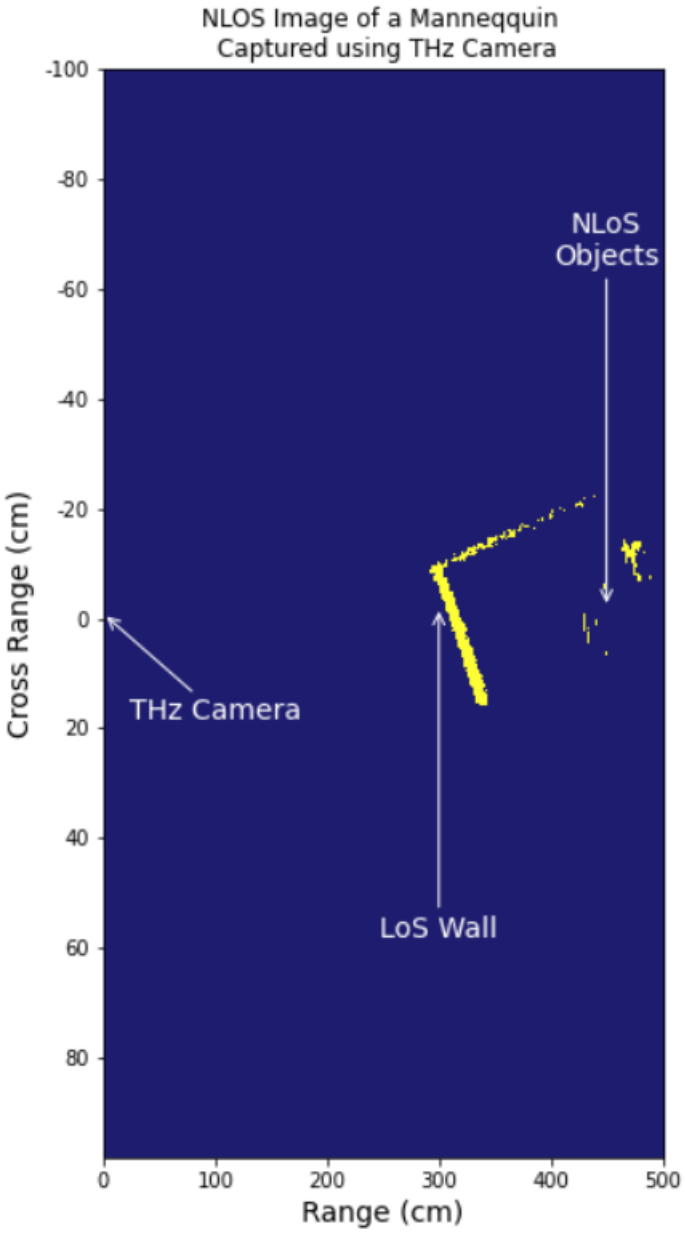

Figure 2-6: Reconstruction of THz image with ghost objects in the NLoS region

As we can see, the NLoS objects, mannequin, fire extinguisher box are seen as if they are behind the wall, instead of in their correct position, the corridor. This is a wrong depiction of the scene. We call the objects behind the walls as ghost objects. A method to solve this problem is represented in chapter 3.

CHAPTER 3

THz NLoS CORRECTION ALGORITHM

The idea now is to correct the scene by solving the problem by using image processing techniques. As mentioned in the earlier chapters, we are now to use the 2-dimensional representation of the 3D reconstruction and correct for the wrong positions of the ghost objects. The problem of detecting LoS objects in a scene/image has been well understood and solved many times using a multitude of techniques in the field of computer graphics. One such technique is ray casting from a point source to detect whether the cast ray is hit or missed. For that and to achieve proper correction, we move the problem from the RF domain into the image processing domain where every image is a 2-dimensional matrix of numbers represented by various intensities. The smallest unit of an image is termed to be a pixel.

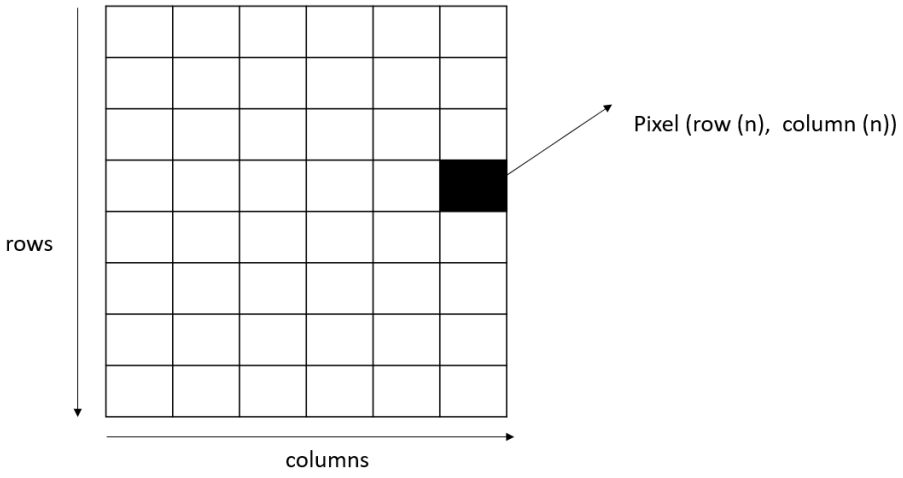

Figure 3-1: Representation of an image as a two-dimensional matrix

Every image coming out of our THz imaging system is considered a matrix formed by the 2D cross section in the azimuth and elevation directions of the 3D image To walk through the correction procedure, a simulated test case is considered where an object is

around a corner from the viewport of the THz camera in front of a wall. A scan is performed in the azimuth and elevation directions to capture an NLoS image .

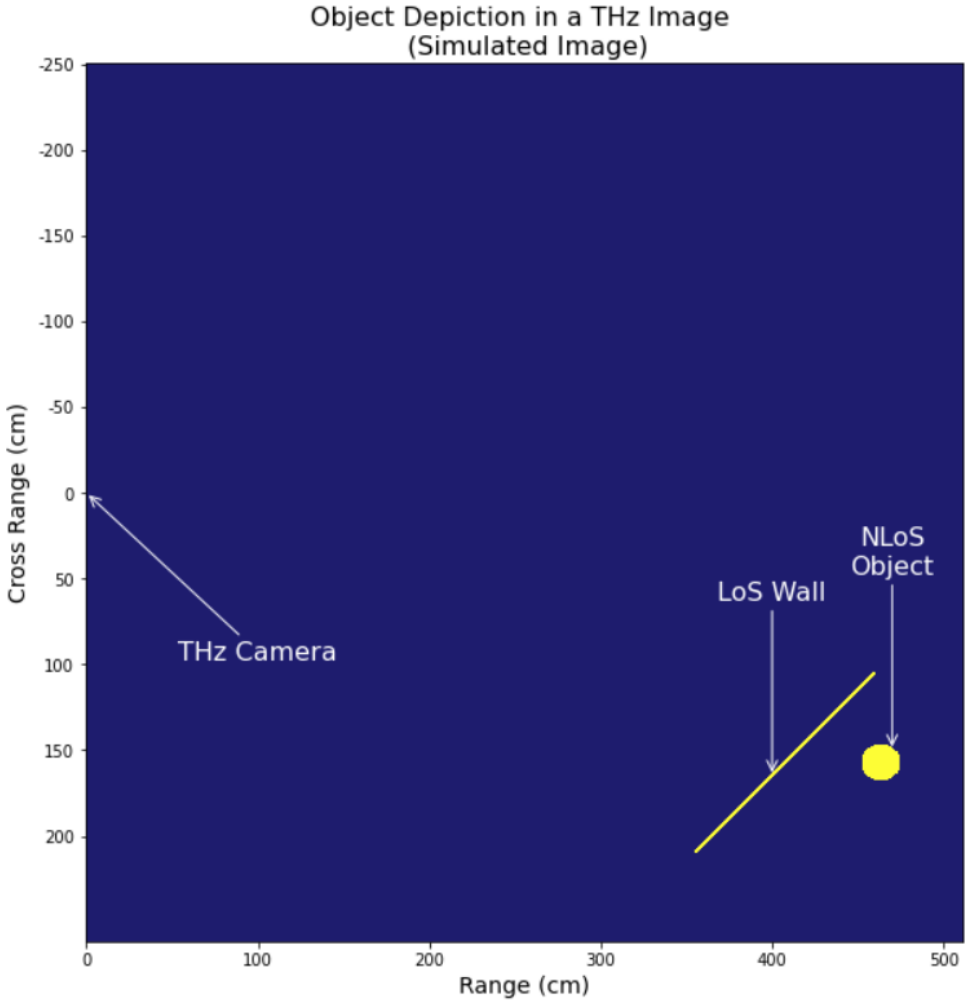

Figure 3-2: 2D cut of a 3D THz image with an object in the NLoS region of the camera.

3.1 Pre-processing

We collect the raw data from the MATLAB script, apply IFT, and generate a 3D reconstruction of the scene captured by the THz camera. Before correction can be applied we convert this information into a 2D image as it can be seen in Figure 3-2. Before each

image is processed any further, we apply a thresholding step to the image. i.e., a pixel intensity above which the information in the image is to be retained is chosen and the rest of the information is considered as free space. This aids in removing any noise due to 1) receiver intrinsic noise and 2) clutter noise (multipath diffuse scattering) and helps in accurate reconstruction of the scene.

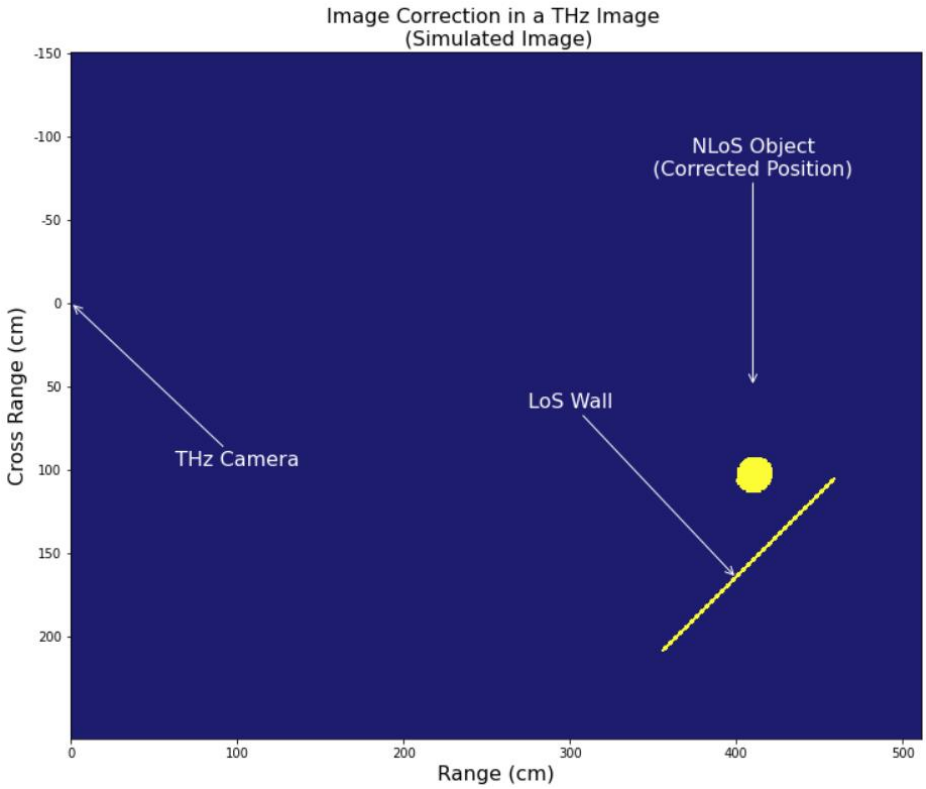

Figure 3-3: Example of a THz image after applying mirror folding.

In this figure, a corrected representation of figure 3-2 is shown. Here the NLoS object has been mirrored around the LoS wall. We can see that the LoS wall is at a distance from the imaging system, and the NLoS object is close to the LoS surface.

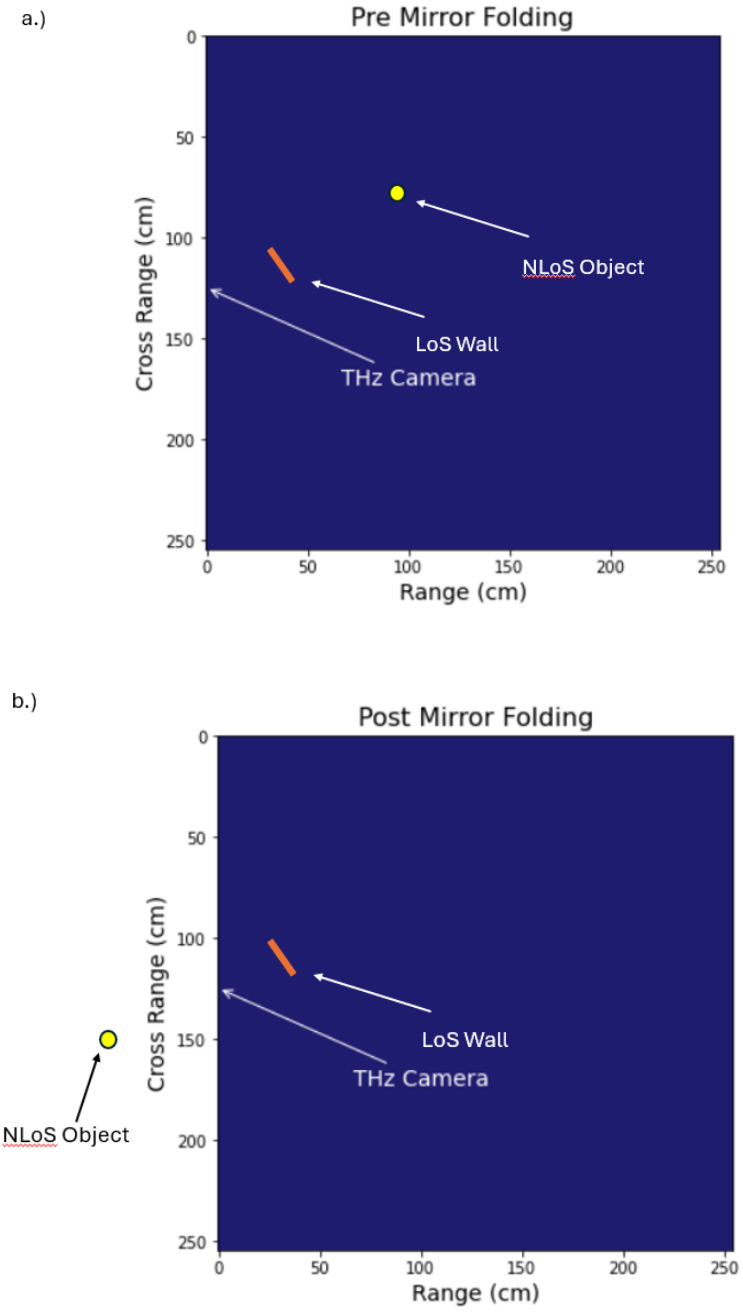

Figure 3-4: a.) Example of a THz image with an object far away from the LoS surface pre-folding. b.) NLoS object out of the bounds of image after mirroring.

In cases where the LoS surfaces are near the imaging system and when the NLoS objects are farther away from the LoS surface, a problem may arise i.e., after mirroring since the

NLoS object will be placed at the same distance on the opposite side of the LoS surface, the position of NLoS objects could be determined incorrectly and it may be placed outside the bounds of the image. To solve this problem we increase the size of the THz image (upscaling) by preserving the locations of all objects in the image so that we can properly mirror the NLoS object without the problem of it being outside the bounds of the image.

3.1.1 Point Selection for Classification

Once a suitable threshold is selected, we scale the canvas to a size that is 3 times larger in both height and size than the original dimensions. We then create a new canvas with those dimensions and carefully fill all the pixels that were above the selected threshold in such a way that the original image is at the center of the new canvas with enough space in all directions to be able to mirror the object to its right position. We also created a memory map of the location of the pixels in terms of their row and column indices. This set of points is called the *region of interest* and is used later down the pipeline.

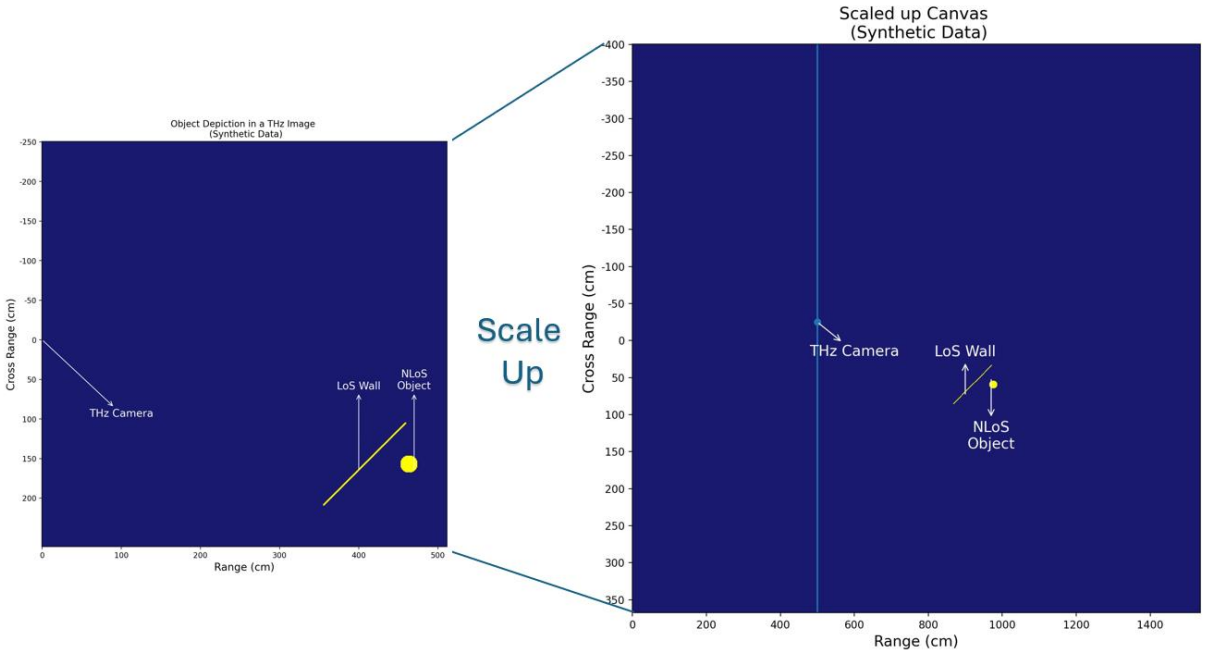

Figure 3-5: A THz image represented on an upscaled canvas before applying correction.

3.1.2 Classification by Ray Casting

Ray Casting is the basis for most modern rendering solutions that use a geometric algorithm for ray tracing. The idea of ray casting is simple in the sense that geometric rays are traced along straight-line paths with the eye of the observer as the point of origin for these rays.

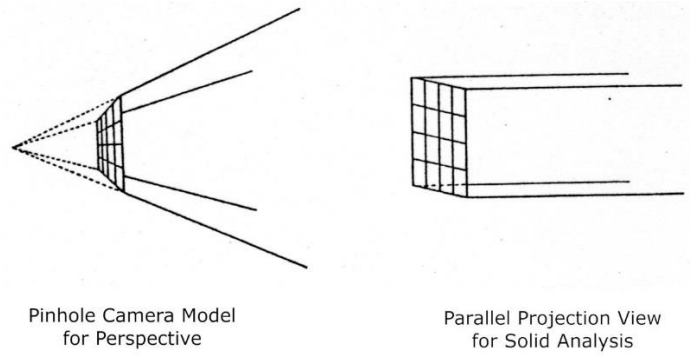

Figure 3-6: Idea of Ray Casting for a Pin Hole Camera

(By Scott Roth - Own work, CC BY-SA 4.0)

Ray casting is a reliable and extensive method [5] for faster image generation and 3-dimensional scene rendering although it is not the purpose that it is used for here in this work. The principles of ray casting applied here are like those applied in video games specifically to render objects that are only directly in front of the first-person character. All the assets behind the direct line of sight objects are not rendered to optimize the memory used by the game. Wolfenstein-3D is one such game that greatly utilizes the ray-casting technique to render scenes.

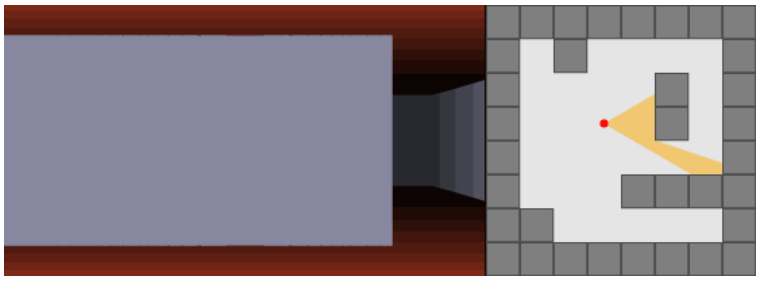

Figure 3-7: Ray casting in a game engine (by Lucas Vieira - public domain)

In this case, the position of the THz camera depicted by a solid red line in the figures shown previously is a singular point in the 2-dimensional space and serves as the source or the viewpoint from which the rays are to be rendered. We now make use of basic trigonometric principles to find the angle between different points in the region of interest and create buckets of points with each bucket labeled by its angle using the algorithm as follows:

for co-ordinate in region-of-interest:

find angle with respect to the source:

if the angle has already been detected:

add the point to the bucket

if there is no bucket:

create a new bucket and add that point to the bucket

This process is analogous to casting rays in an image-rendering situation. Once the process of scanning across all the points in the region of interest is complete and all points have been placed into their respective buckets, we perform a simple sorting operation to place the points in an increasing order of their distance in terms of columns from the source point.

For co-ordinate in each-bucket:

sort by column index

Based on this operation, the first point in every bucket can be termed to be the closest or first point seen by the ray cast from the source and be termed to be a LoS object. We then set a distance threshold based on the estimated thickness of walls in several pixels and classify the rest of the points in the object as NLoS objects. Upon completion of this operation, we are left with two sets of points, called the LoS points and the NLoS points.

a.)

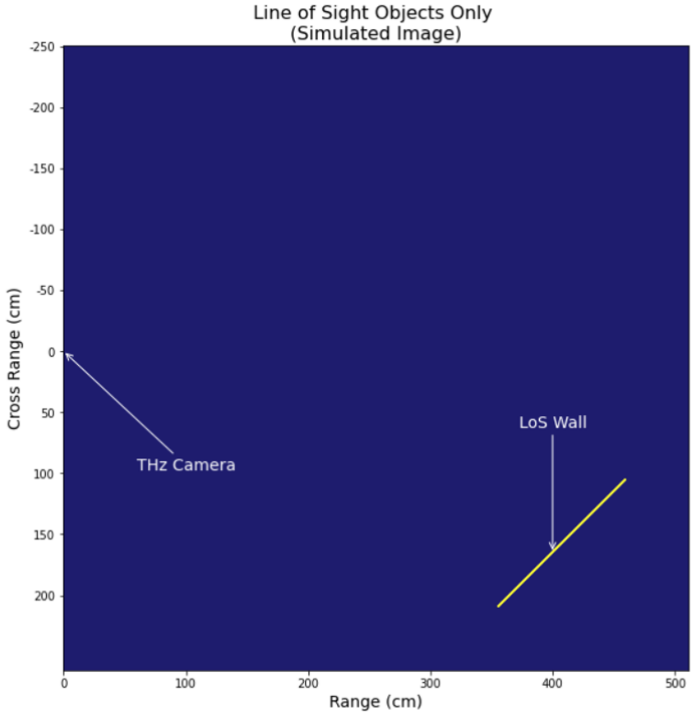

b.)

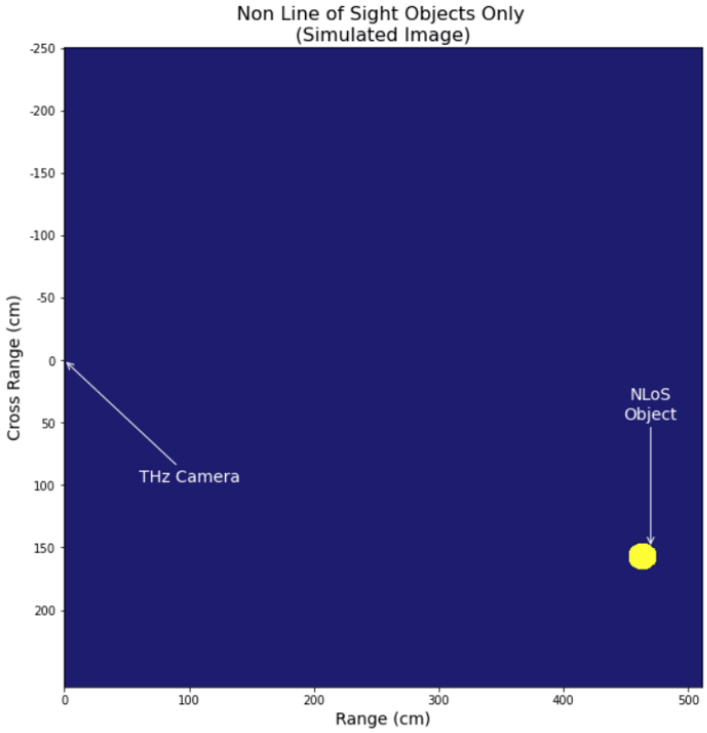

Figure 3-8: a.) THz showing LoS wall only. b.) THz image showing NLoS object only.

3.2 Mirror Detection

Using the information about the LoS points in our canvas, we can now proceed to mirror surface detection. This work assumes perfect reflections and thus only focuses on modeling surfaces as plane mirrors i.e., straight line reflection. We used the knowledge acquired from the results of works [6] and [7] and applied it to our problem.

3.2.1 Edge Detection

Edge detection is a fundamental tool in image processing advantageous in the fields of machine and computer vision. It involves the identification of edges, and discontinuities in brightness or intensity within images using a multitude of techniques. Canny edge detection is a popular multistep edge detection technique that is useful for detecting a wide range of edges. The Canny Edge detector works by applying a Gaussian filter to smoothen the image and reduce noise as its first step. An intensity gradient calculation is performed to detect the direction of the edge propagation followed by a gradient magnitude thresholding. A second thresholding operation is performed, before finalizing the edges by hysteresis tracking.

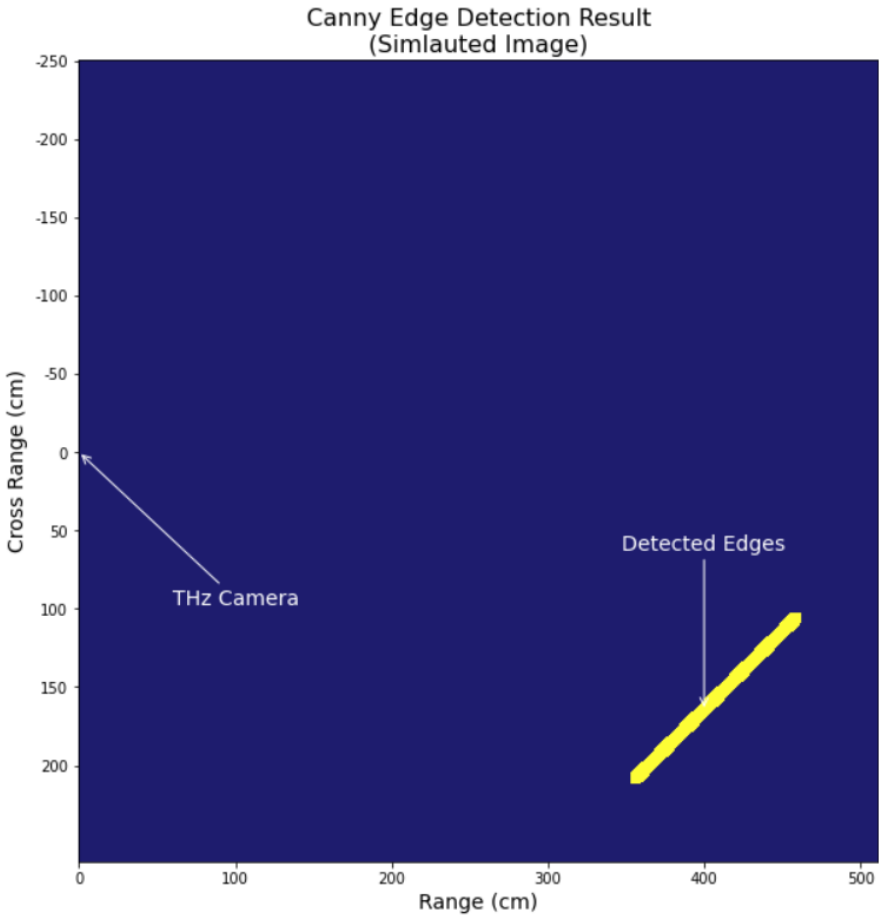

Figure 3-9: Output from canny edge detection.

An implementation of the Canny edge detector is provided by the OpenCV python package which is used here to obtain the edges from the LoS points. The edge information is available as a 2D matrix result which can then be used in the following stages of the algorithm.

3.2.2 Probabilistic Hough Line Transform

The edge information obtained in the previous stage can be used to extract the information about what parts of the image constitute a linear segment which can be used to model the mirroring surface. For this, we use a known line detection method called

Hough Transform. A line in a 2-dimensional space can be represented using a mathematical expression defined by

$$y = mx + b$$

where m is the slope of the line and b is the y-intercept. To avoid errors caused by odd values of slope caused due to vertical lines, the line shall be represented as

$$r = x\cos\theta + y\cos\theta$$

Where r is the perpendicular distance from the origin to a point on the line and θ is the angle between the x-axis and the line connecting the origin with the closest point. Defining a line in two such methods gives us an opportunity to look at the possible set of lines in both the image space where the equation of a line is in y, x space and in a parameter, space defined by r, θ.

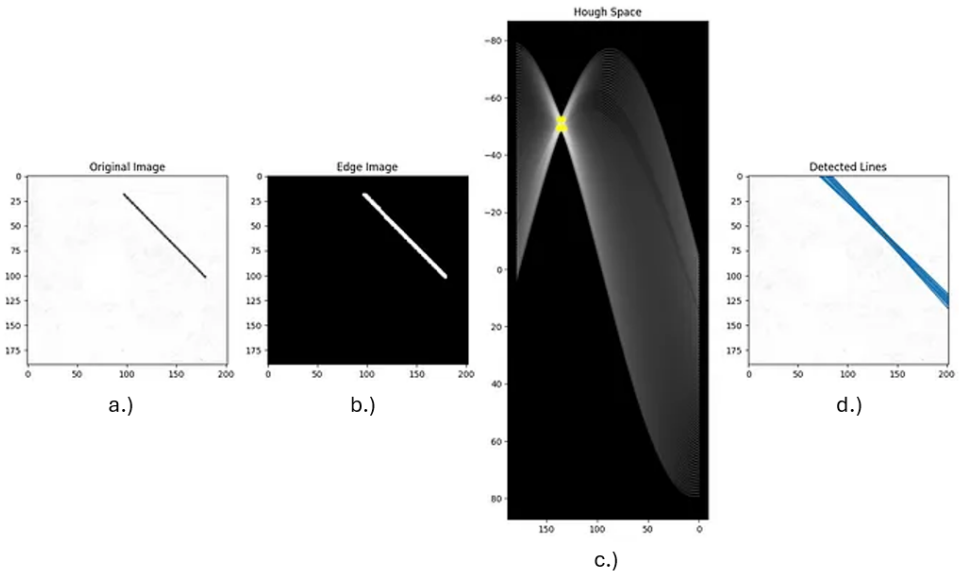

Figure 3-10: Hough Transform in different stages of line detection a.) Source image with a line in it. b.) Canny edge detection applied to the image containing a line. c.) Representation of edges in the Hough space. d.) Lines detected by the Hough transform.

A single point in the image space is represented by a sinusoid in the r, θ space. For each point we obtain in the Canny edge detection step, a sinusoid is formed as shown in the "Hough Space" subplot in the figure above. An accumulator array is created for each point in the edge set and a voting scheme is applied over the accumulator array. The accumulation happens across the sinusoid. Every intersection means an additional point falling onto a line. This process is abstracted by the OpenCV's implementation of the Hough Transform P method which directly gives us the endpoints of the detected line.

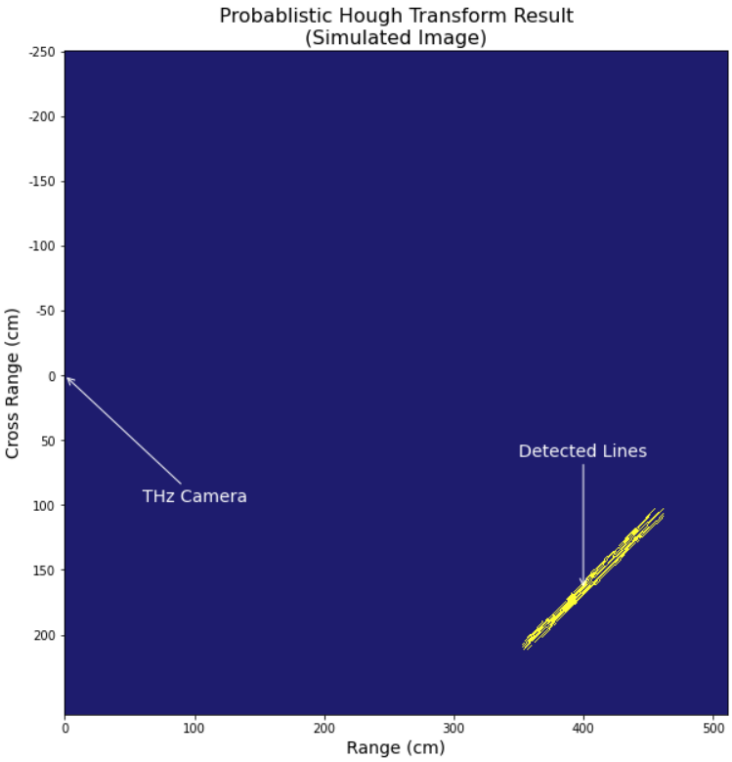

Figure 3-11: Multiple lines detected by applying probabilistic Hough line transform using edges from Canny edge detector.

We obtain more than one line for a given surface and we need to reduce this solution set to one. Therefore, a secondary accumulation method is applied over the set of endpoints obtained. This accumulation process takes each point and finds the angle

between the source point which is the location where the THz camera is located.. With each line having two endpoints, we have two angles, θ_1 and θ_2 namely starting and ending angles. I created an accumulator vector with 180 spaces, one for each angle, and initialized with arrays containing zeros. For each range between the starting and ending angle, we fill the respective position with the value one. We detect the longest sequence of ones and set it as the starting and ending points of our detected line ergo, the starting and ending points of our surface.

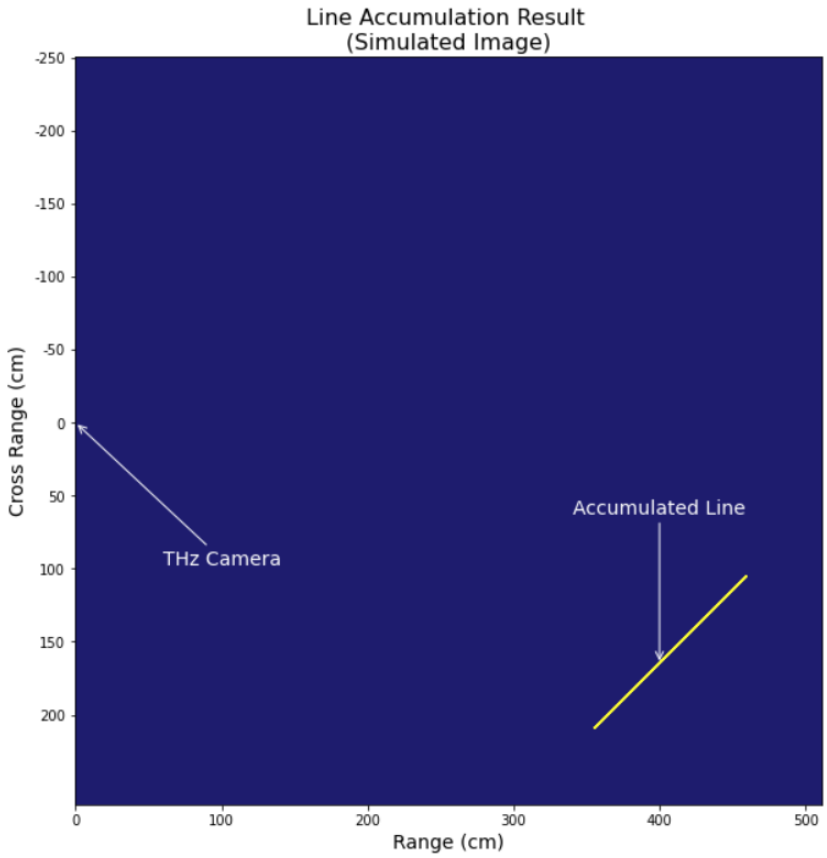

Figure 3-12: Accumulated line from Hough line transform output.

3.3 Forming Hierarchies for NLoS Objects

Now that we know the starting and ending points of the mirroring surface, we can associate all the points in the NLoS region to that surface. This is programmatically achieved by the process of creating a Mirror object with all the NLoS points set as a parameter to that object. This process of associating the coordinates of the NLoS points to the surface they are to be mirrored about can be termed Hierarchy formation.

3.4 Geometric Mirroring of NLoS Objects

Although this is a simple geometric transformation and needs to be performed carefully, it is important `that there could be multiple mirroring surfaces that have been detected with multiple objects behind them. The process of finding the mirrored position of a point about a line is as follows. Given we know the starting and ending positions of the mirrored surface, they can be used to find the equation of the surface.

Let the co-ordinate of the starting point of the mirror surface be ($x1$, $y1$) and that of the ending point be ($x2$, $y2$) the equation of the line joining these two points can be found as

$$\frac{y - y_1}{y_2 - y_1} = \frac{x - x_1}{x_2 - x_1}$$

Comparing the outcome of this equation with another standard equation

$$ax + by + c = 0$$

We can find the coefficients a, b, c and use them to find the mirrored position x, y of an NLoS point x3, y3 as

$$\frac{-2(ax_3 + by_3 + c)}{a^2 + b^2} = \frac{y - y_3}{b} = \frac{x - x_3}{a}$$

With x_1, y_1 and x_2, y_2 being the endpoints of the mirroring surface and x_3, y_3 being the points in the NLoS region, the process of mirroring is repeated to obtain a mirrored point set.

3.5 Addressing the Multi-Bounce Scenarios

In the real world more than one reflecting surface may be present and reflecting surfaces may be present within the NLoS region of the imaging system. This may lead to multiple backscatters causing a secondary ghosting of the NLoS object. Below is one such example described in [2]

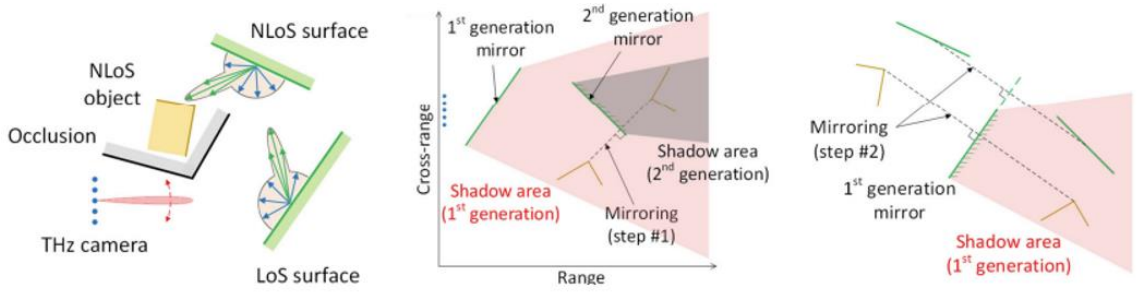

Figure 3-13: A simulated scenario containing a reflective surface within the NLoS region of the first surface [2]

Such a scenario requires multiple levels of corrections. It can be observed that the NLoS surface acts as a secondary mirror and the ghost object behind it needs to be corrected first and then the entire geometry needs to be corrected around the primary mirror.

3.6 Applying the Algorithm for Multi Bounce Scenario

We use the example scenario presented in [1] as an example to demonstrate the application of this algorithm for a multibounce scenario.

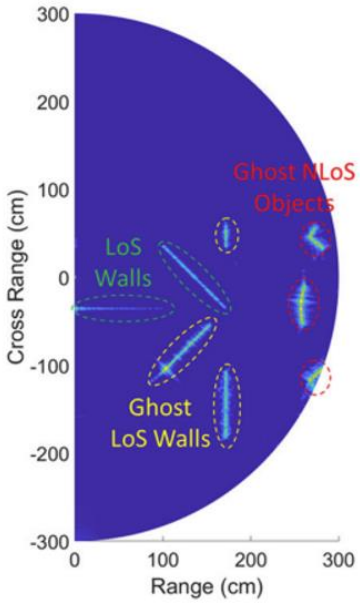

Figure 3-14: A simulated case with more than one bounce [2]

As the first step in our pipeline, we apply thresholding and scaling. A preliminary LoS and NLoS classification is performed.

a.)

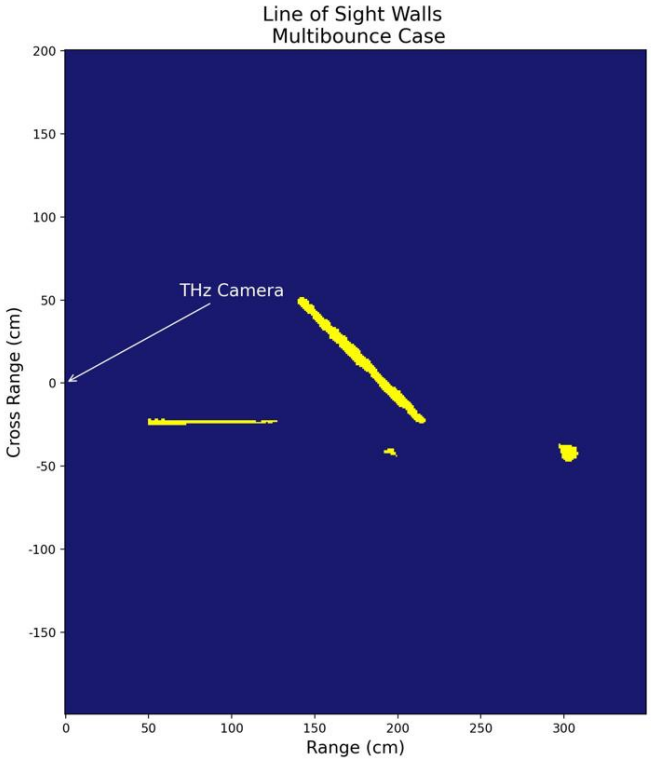

b.)

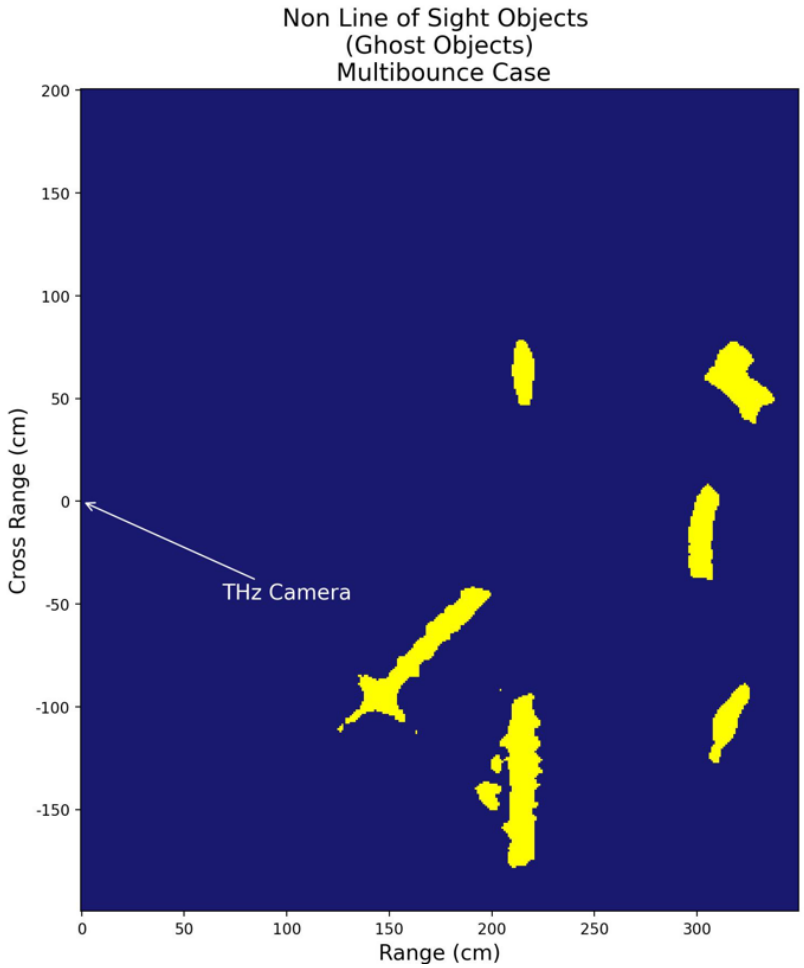

Figure 3-15: Top-level classification of the multibounce scenario. a.) LoS walls as seen from the THz camera. b.) NLoS objects hidden behind the LoS walls.

In figure 3.15 we can observe multiple ghost objects and we can also see that the are mirroring surfaces in the NLoS region of the LoS surfaces. These mirrors can be called secondary mirrors. Because of the presence of the secondary mirrors, we cannot directly mirror the objects around each mirror and stitch the image together. We must now proceed to the next step of detecting the primary mirrors, accumulating for a single surface, and then grouping the NLoS objects to their respective mirrors, and performing a secondary search in each of the NLoS regions.

This procedure of detecting mirrors, secondary mirrors, tagging individual objects by the mirror, then mirroring the objects around secondary mirrors, mirroring these objects around the direct LoS mirrors in front of the THz camera is automated for a 2-bounce case.

a.)

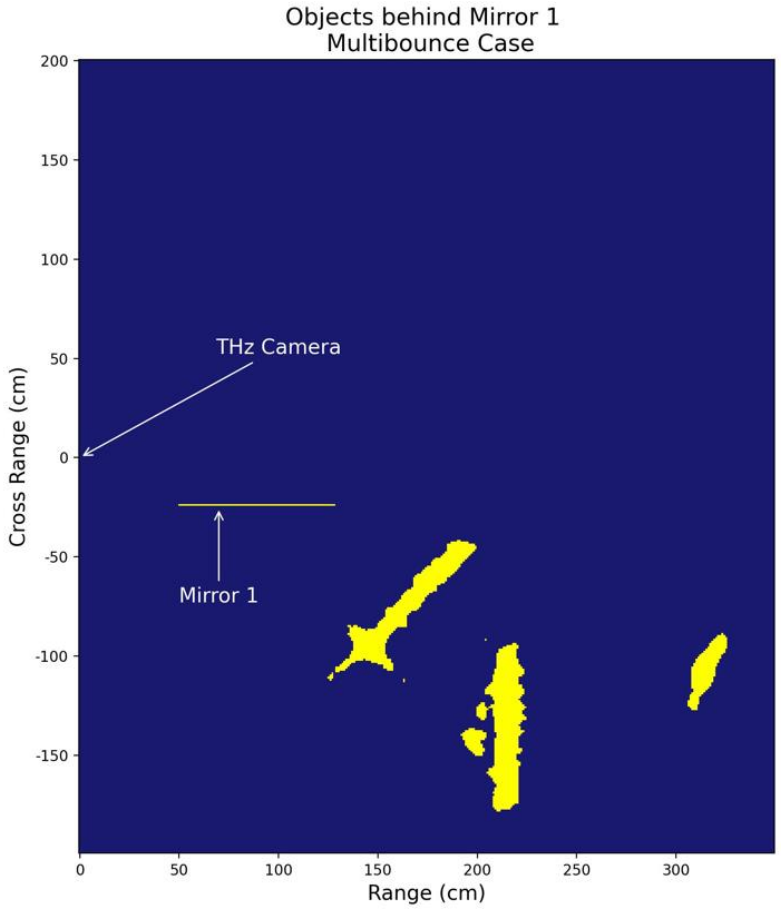

b.)

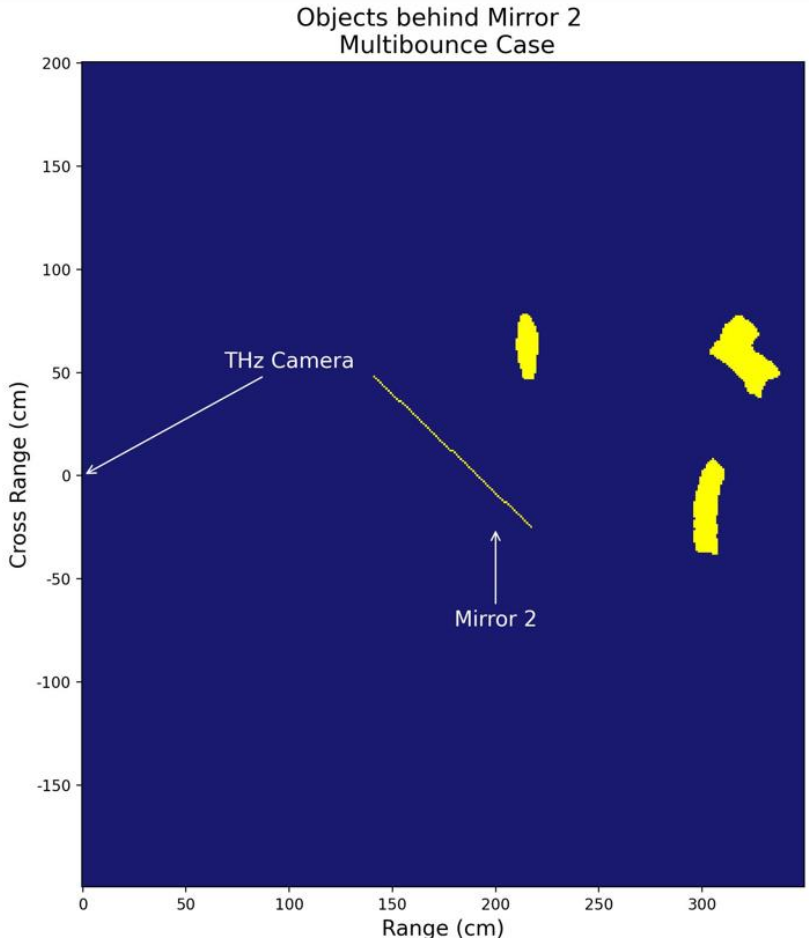

Figure 3-16: Mirror Surface detection and tagging by appropriate mirrors.

a.) NLoS objects behind primary mirror 1 b.) NLoS objects behind primary mirror 2

In figure 3-16, we can see how each of the mirrors and their associated NLoS objects are shown. Each of the mirrors that is detected is allocated a space in the program to store the positions of objects behind it, so that mirroring can be performed later. In sub figure a., we see that there is a secondary mirror in the shadow region or the NLoS region of Mirror 1. The secondary mirror also has objects behind it.

According to our idea of mirror folding, we need to first rotate the objects around the mirrors far from the THz camera i.e., secondary mirrors and then move on to the parent mirrors. We perform a second classification for objects in NLoS region of the first

mirror.

a.)

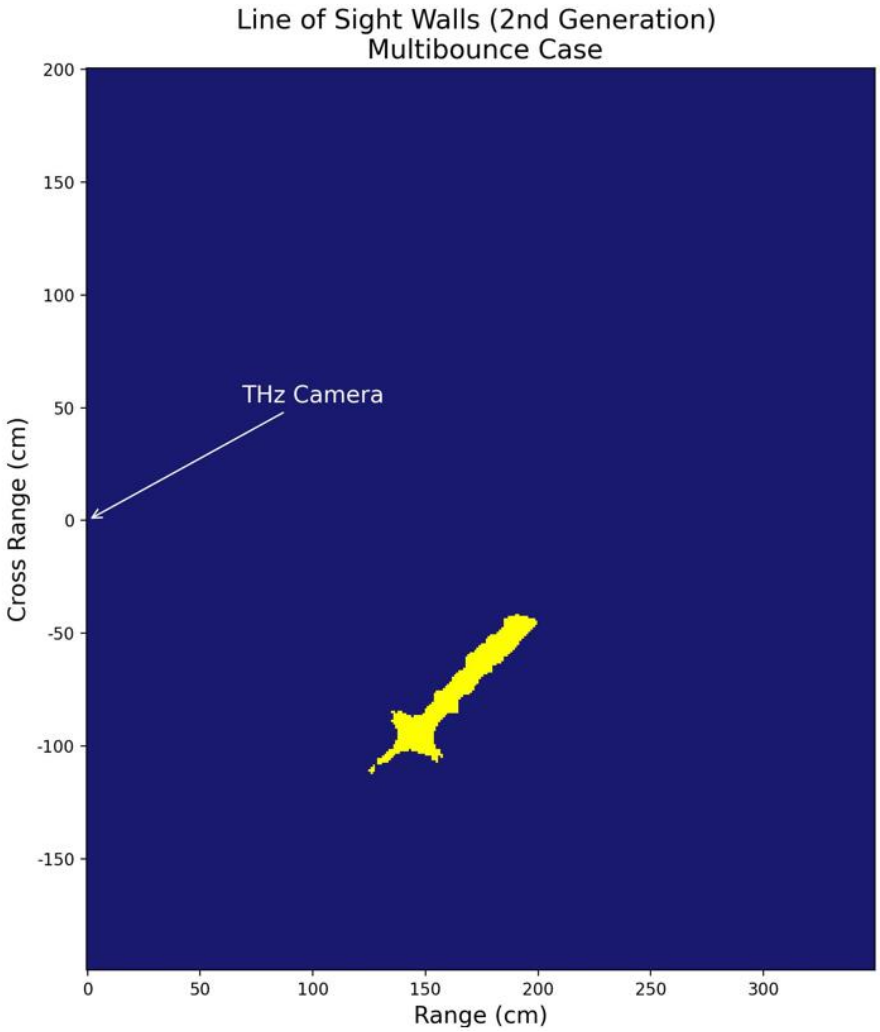
Line of Sight Walls (2nd Generation)
Multibounce Case
THz Camera
Cross Range (cm)
Range (cm)
200
150
100
50
0
-50
-100
-150
0
50
100
150
200
250
300

b.)

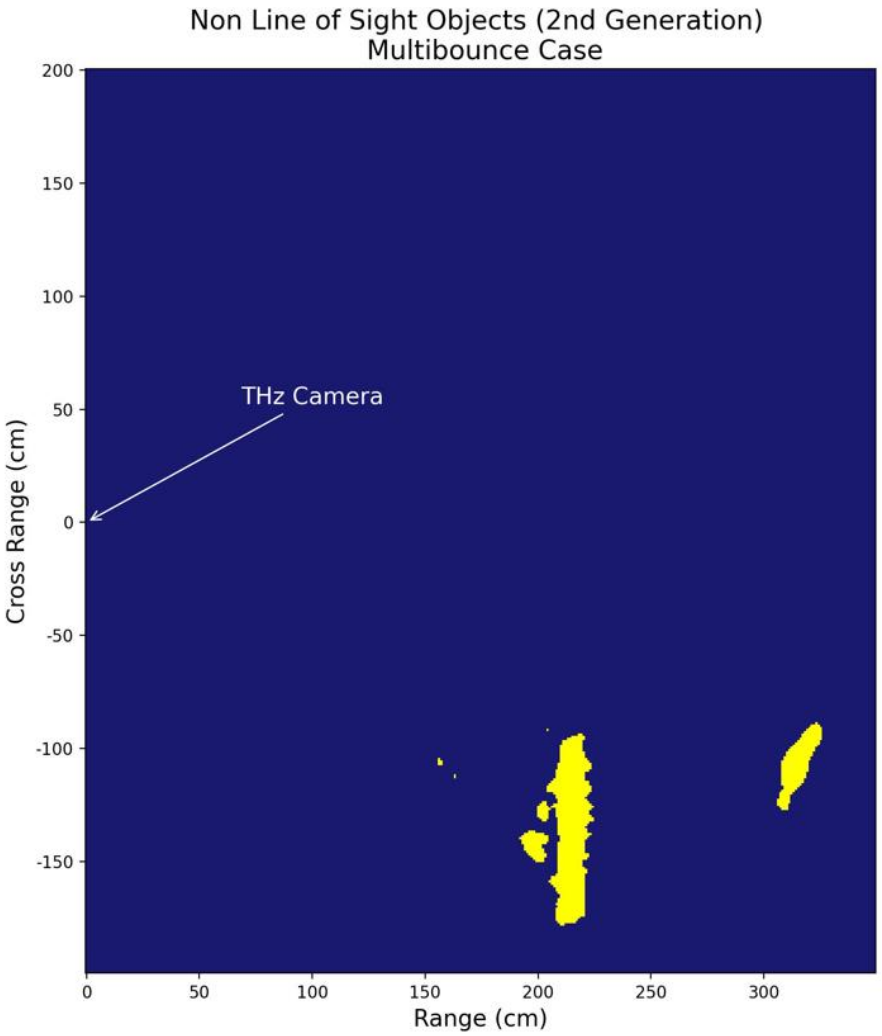

Figure 3-17: Classification in the NLoS region of Mirror 1. a.) LoS mirror found in NLoS region of Mirror 1. b.)NLoS objects behind the secondary mirror.

Edge detection followed by a line accumulation is performed for the secondary mirror like in the single bounce case. The endpoints of the secondary mirror are obtained.

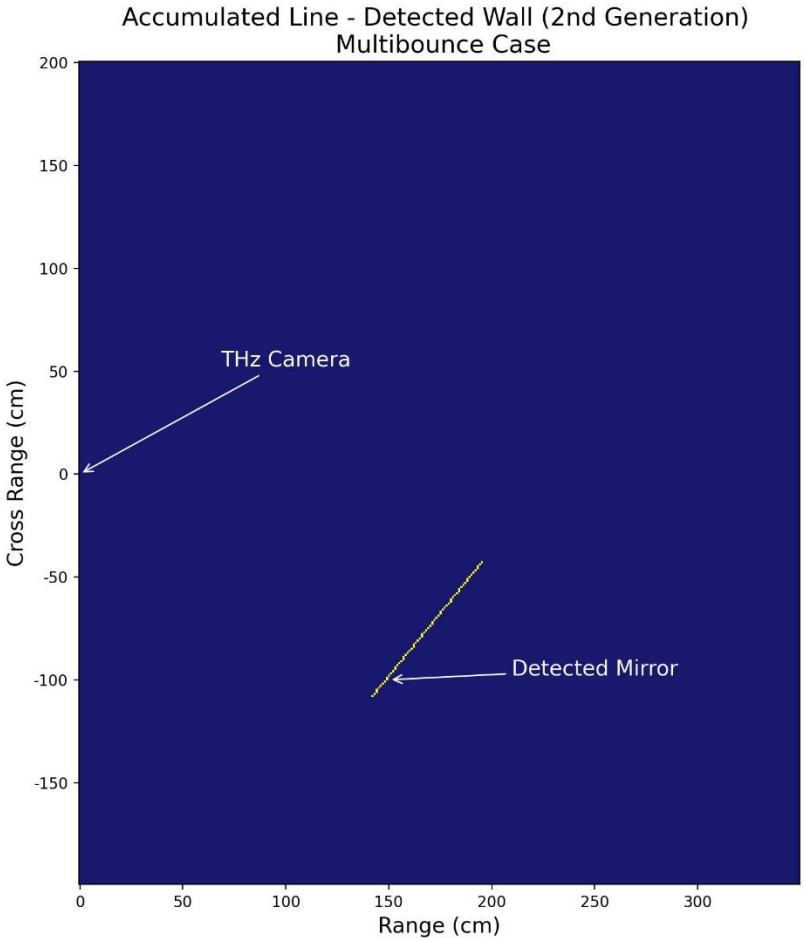

Figure 3-18: Detected mirror in the shadow region of Mirror 1.

It is to be noted that the mirrored points of this secondary reflection are still tagged to their primary mirror. Since there are no other secondary reflections for the other primary LoS surfaces. We start by mirroring the points with a secondary reflection of their new positions.

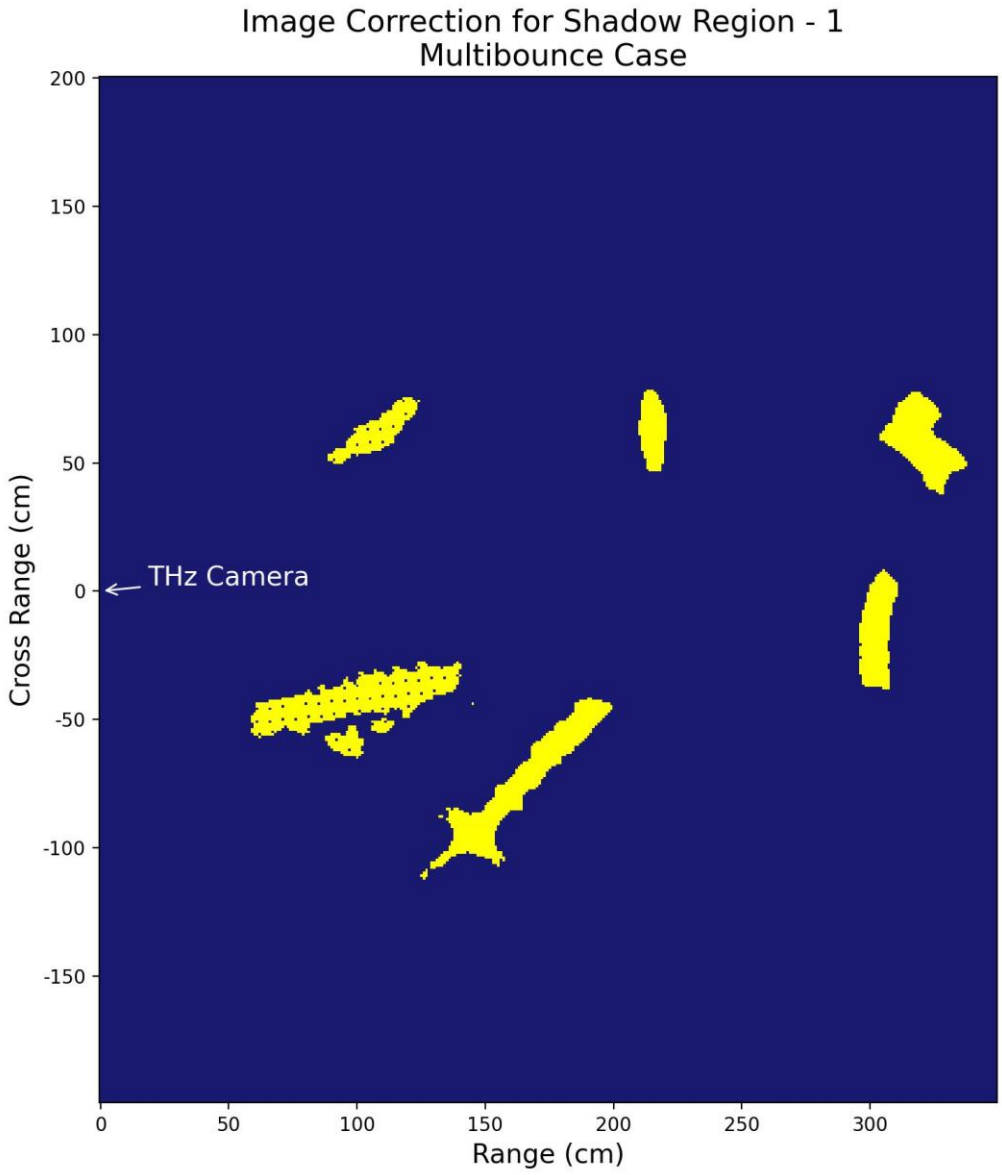

Figure 3-19: Reflecting NLoS objects within the shadow region of Mirror 1.

A final mirror folding is applied to all the points that are tagged initially to the individual mirrors to result in a geometry that represents the actual positions of all the objects.

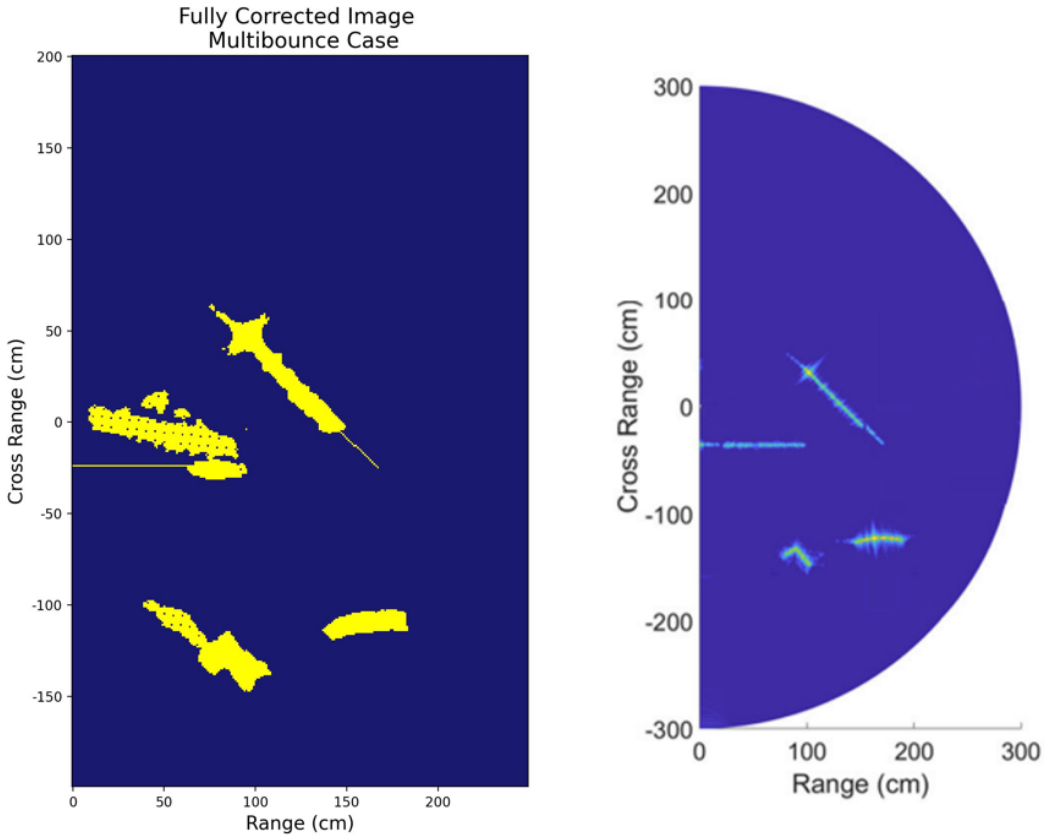

Figure 3-20: Side by Side comparison of the final mirror folding obtained from the implementation of the algorithm and the result presented in [2]

We obtain a near-accurate result to what the original proposal shows. The errors in accuracy can be accounted for by accumulated errors due to improperly mirroring second-generation reflections.

CHAPTER 4

CONCLUSION

4.1 Summary

This work is focused on building a system that functions as raw data in and corrected image out. What this work isn't is that it does not focus on what EM wave techniques are used or their mathematical explanations.

This work begins with an explanation of why and how THz imaging can be leveraged for NLoS imaging and its associated applications. A detailed description of how the imaging setup operates, and how raw data is processed to construct a 3-D scene is discussed. Then, to correct the errors caused by objects being incorrectly depicted as ghost objects, image processing techniques like ray-casting, Hough-line transform, canny-edge detection, are discussed. These image-processing techniques are combined to form a correction algorithm. This correction algorithm is applied to single bounce and multiple bounce scenarios and the results have been presented.

4.2 Conclusions

1. This method is what is known as a post-processing technique where once the data collection is completed, it undergoes multiple preprocessing steps and the image is corrected. The algorithm has been implemented in Python programming language for the ease of rapid iteration. Python is typically considered a slow language. Thus we need to implement the algorithm in a low-level programming language like C or C++ so that it can be used in real time correction.

2. The preprocessing steps are currently handled in two programming languages, MATLAB and Python which makes the entire pipeline slower than usual. A way to eliminate this process would be to implement the IFT pipeline in the raw image handler of the algorithm itself. Once this bottleneck has been eliminated comes the step where we adjust many thresholds used in determining the region of interest determination.
3. The algorithm in its current form is capable of handling reflections caused by mirrors up to two generations; this is achieved by automatically searching through the NLoS objects of the first-generation mirrors for any secondary mirrors. This step can be extended to generations greater than 2 by making necessary parameter changes within the program.
4. As discussed in earlier chapters, THz raw images are 3D in nature formed by plotting the voxels. The current algorithm can be expanded to 3D domain by implementing edge and line detections for 3D surfaces and extending the geometric mirroring in linear domain to 3 dimensions.
5. One of the still manual steps in the mostly automated solution to THz image correction is threshold selection, which is carried forward into several steps down the pipeline. This can be automated by estimating the average intensity of the voxels in the 3D image and finding its corresponding value in the 2D cross-section.
6. Since most of the image processing operations are vector-based, more performance can be achieved through performing parallel processing.

Overall, this algorithm can be successfully used to correct THz images up to 2 generations with the exception of accuracy errors for 2 bounce cases. As one can see, in

figure 3.20, the image on the right is cleaner than the one that has been corrected by the automated algorithm. It is because the points that are to be reflected were hand-picked carefully and were manually placed in their correct positions. As we can see from the image on the left, some of the objects are not correctly placed in their positions. This is because of the mirroring errors that occurred in the secondary mirror. These errors got carried forward to the primary mirror where the error increased. This can be eliminated by carefully tuning the mirroring algorithm.

REFERENCES

[1]. Y. Cui and G. C. Trichopoulos, "3D Non-Line-of-Sight Terahertz Imaging Using Mirror Folding," 2022 United States National Committee of URSI National Radio Science Meeting (USNC-URSI NRSM), Boulder, CO, USA, 2022, pp. 89-90, doi: 10.23919/USNC-URSINRSM57467.2022.9881411.

[2]. Cui, Y. (2022).” Non-Line-of-Sight Imaging Methods Using Terahertz Waves”, Arizona State University (ProQuest)

[3]. M. Aladsani, A. Alkhateeb, and G. C. Trichopoulos, "Leveraging mm-Wave Imaging and Communications for Simultaneous Localization and Mapping," ICASSP 2019 - 2019 IEEE International Conference on Acoustics, Speech and Signal Processing (ICASSP), Brighton, UK, 2019, pp. 4539-4543, doi: 10.1109/ICASSP.2019.8682741.

[4]. S. k. Doddalla and G. C. Trichopoulos, "Non-Line of Sight Terahertz Imaging from a Single Viewpoint," 2018 IEEE/MTT-S International Microwave Symposium - IMS, Philadelphia, PA, USA, 2018, pp. 1527-1529, doi: 10.1109/MWSYM.2018.8439239.

[5]. Roth, S. (1982) “Ray Casting for Modeling Solids.” Computer Graphics and Image Processing, 18, 109-144.http://dx.doi.org/10.1016/0146-664X(82)90169-1

[6]. J. Canny, "A Computational Approach to Edge Detection," in IEEE Transactions on Pattern Analysis and Machine Intelligence, vol. PAMI-8, no. 6, pp. 679-698, Nov. 1986, DOI: 10.1109/TPAMI.1986.4767851.

[7]. Richard O. Duda and Peter E. Hart. 1972. “Use of the Hough transformation to detect lines and curves in pictures”. Communications. ACM 15, 1 (Jan. 1972), https://doi.org/10.1145/361237.361242

[8]. D. B. Lindell, G. Wetzstein, and V. Koltun, "Acoustic Non-Line-Of-Sight Imaging," 2019 IEEE/CVF Conference on Computer Vision and Pattern Recognition (CVPR), Long Beach, CA, USA, 2019, pp. 6773-6782, doi: 10.1109/CVPR.2019.00694.

[9]. Andre Beckus, Alexandru Tamasan, and George K. Atia. 2019. “Multi-Modal Non-Line-of-Sight Passive Imaging.” Trans. Img. Proc. 28, 7 (July 2019), https://doi.org/10.1109/TIP.2019.2896517.

[10]. Nicolas Scheiner, Florian Kraus et.al., "Seeing Around Street Corners: Non-Line-of-Sight Detection and Tracking In-the-Wild Using Doppler Radar" CVPR 2020

[11]. P. Setlur, T. Negishi, N. Devroye and D. Erricolo., Multipath Exploitation in Non-LOS Urban Synthetic Aperture Radar, in IEEE Journal of Selected Topics in Signal Processing, vol. 8, no. 1, pp. 137-152, Feb. 2014.

[12]. M. Lecci, P. Testolina, M. Polese, M. Giordani and M. Zorzi, "Accuracy Versus Complexity for mm-Wave Raytracing: A Full Stack Perspective," in IEEE Transactions on Wireless Communications, vol. 20, no. 12, pp. 7826-7841, Dec. 2021, doi: 10.1109/TWC.2021.3088349.

[13]. T. Maeda, Y. Wang, R. Raskar, and A. Kadambi, "Thermal non-line-of-sight imaging" in 2019 IEEE International Conference on Computational Photography (ICCP). IEEE, 2019, pp.

[14]. X. Liu, S. Wei, J. Wei, J. Shi, X. Zhang and Y. Li, "Non-Line-of-Sight Millimeter-Wave Radar 3-D Sparse Reconstruct via MSSTV Method," 2022 IEEE 9th International Symposium on Microwave, Antenna, Propagation and EMC Technologies for Wireless Communications (MAPE), Chengdu, China, 2022, pp. 424-427, doi: 10.1109/MAPE53743.2022.9935195.

[15]. S. Guo, Q. Zhao, G. Cui, S. Li, L. Kong, and X. Yang, "Behind corner targets location using small aperture millimeter wave radar in NLoS urban environment" IEEE Journal of Selected Topics in Applied Earth Observations and Remote Sensing, vol. 13, pp. 460-470, 2020.

[16]. S. Wei, J. Wei, X. Liu, M. Wang, S. Liu, F. Fan, X. Zhang, J. Shi, and G. Cui, "Nonline-of-sight 3-d imaging using millimeter-wave radar", Nonline-of-sight 3-d imaging using millimeter-wave radar pp 1-18, 2021.

[17]. Julian Iseringhausen and Matthias B. Hullin. 2020. "Nonline-of-sight Reconstruction Using Efficient Transient Rendering. ACM Trans. Graph. 39, 1, Article 8 (February 2020)", 14 pages. https://doi.org/10.1145/3368314.

[18]. Bin Wang et al, Non-Line-of-Sight Imaging with Picosecond Temporal Resolution, Physical Review Letters (2021). DOI: 10.1103/PhysRevLett.127.053602

[19]. J. Palacios, G. Bielsa, P. Casari and J. Widmer, "Communication-Driven Localization and Mapping for Millimeter Wave Networks," IEEE INFOCOM 2018 - IEEE Conference on Computer Communications, Honolulu, HI, 2018, pp. 2402-2410.

[20]. M. Grzegorzek, C. Theobalt, R. Koch, and A. Kolb, Time-of-Flight and Depth Imaging: Sensors, Algorithms and Applications. 1st edition. Berlin, Heidelberg, Germany: Springer, 2013.

[21]. C. Jansen et al., “Diffuse Scattering from Rough Surfaces in THz Communication Channels,” IEEE Transactions on Terahertz Science and Technology, vol. 1, no. 2, pp. 462-472, Nov. 2011.

[22]. P. Rangarajan and M. P. Christensen, “Imaging hidden objects by transforming scattering surfaces into computational holographic sensors,” in Imaging and Applied Optics 2016, OSA Technical Digest (Optical Society of America, 2016), paper CTh4B.4.

[23]. Takahiro Sasaki, Erich N. Grossman, and James R. Leger, "Estimation of the 3D spatial location of non-line-of-sight objects using passive THz plenoptic measurements," Opt. Express 30, 41911-41921 (2022)

[24]. Liu, X., Guillén, I., La Manna, M. et al. Non-line-of-sight imaging using phasor-field virtual wave optics. Nature 572, 620–623 (2019). https://doi.org/10.1038/s41586-019-1461-3

[25]. Liu, X., Bauer, S. & Velten, A. Phasor field diffraction based reconstruction for fast non-line-of-sight imaging systems. Nat Commun 11, 1645 (2020). https://doi.org/10.1038/s41467-020-15157-4

[26]. Nam, J.H., Brandt, E., Bauer, S. et al. Low-latency time-of-flight non-line-of-sight imaging at 5 frames per second. Nat Commun 12, 6526 (2021). https://doi.org/10.1038/s41467-021-26721-x

[27]. T. Maeda, Y. Wang, R. Raskar, and A. Kadambi, "Thermal Non-Line-of-Sight Imaging," in Proc. 2019 IEEE Int. Conf. Comput. Photography (ICCP), 2019, pp. 1-11.

[28]. Y. He, D. Zhang, Y. Hu and Y. Chen, "Non-line-of-sight Imaging with Radio Signals," 2020 Asia-Pacific Signal and Information Processing Association Annual Summit and Conference (APSIPA ASC), Auckland, New Zealand, 2020, pp. 11-16.

[29]. A. Kadambi, H. Zhao, B. Shi, and R. Raskar, "Occluded Imaging with Time-of-Flight Sensors," ACM Trans. Graph., vol. 35, no. 2, pp. 15:1–15:12, 2016. [Online]. Available: https://doi.org/10.1145/2836164

[30]. Velten, A., Willwacher, T., Gupta, O. et al. Recovering three-dimensional shape around a corner using ultrafast time-of-flight imaging. Nat Commun 3, 745 (2012). https://doi.org/10.1038/ncomms1747

[31]. Liu, M., Liu, H., He, X. et al. Research Advances on Non-Line-of-Sight Imaging Technology. J. Shanghai Jiaotong Univ. (Sci.) (2024) https://doi.org/10.1007/s12204-023-2686-8

APPENDIX A

MAXIMUM UNAMBIGIOUS RANGE OF A RADAR

The maximum unambiguous range of a system is defined as the maximum distance that the radar energy can travel from the source to the target and back to the source between pulses and still produce reliable information. Also known as the maximum unambiguous detectable range it is given by the formula $\frac{C_0}{2\Delta f}$ where Δf is frequency step according to the sampling theorem. Since the maximum unambiguous range determines the distance at which the objects in a NLoS image can be resolved, the frequency step is carefully selected so that objects of the size of a few centimeters can be resolved between the distance of ~1m-2m in the imaging experiments.